Not all DEMs are equal: An evaluation of six globally available 30 m resolution DEMs with geodetic benchmarks and LiDAR in Mexico

This is a non-peer reviewed preprint submitted to EarthArXiv and currently under review in *Remote Sensing of Environment*.

Dr. Jaime J. Carrera-Hernandez (jaime-carrera@geociencias.unam.mx), Twitter: JaimeHydro

Not all DEMs are equal: An evaluation of six globally available 30 m resolution DEMs with geodetic benchmarks and LiDAR in Mexico

J. J. Carrera-Hernández[a,*]

[a]Centro de Geociencias, UNAM. Blvd. Juriquilla 3001, Querétaro, México. CP 76230

Abstract

This work assesses the vertical accuracy of eight Digital Surface Models (DSMs) currently available for Mexico (LiDAR, ALOS AW3D30 V2 and V3, ASTER GDEM V2 and V3, SRTM, NASADEM and Mexico's Continuous Elevation Model (CEM)). The AW3D30, ASTER GDEM, SRTM and NASADEM DSMs cover nearly the entire globe and can be downloaded at no cost, while the LiDAR and CEM DSMs are distributed by Mexico's Institute of Geography and Statistics (INEGI). The accuracy of these DSMs is assessed by considering: 1) benchmarks as reference data at the national level, and 2) LiDAR DSM as reference data on six different zones with variability in slope, vegetation cover and elevation. Using geodetic benchmarks as reference elevation on those areas covered by LiDAR (A_{LiDAR}=370,200 km^2, n_{bench}=24,175), it was found that LiDAR has the best vertical accuracy of all DSMs considered ($\text{MAE}_{\text{LiDAR}}=1.96$), which is why it was used as reference elevation to develop seven Difference of DEMs (DoDs) with the remainder DSMs. Using $n_{\text{cells}}=350 \times 10^6$ for the aforementioned comparisons, it was found that the vertical accuracy of AW3D30 V2 and V3 is similar (MAE=2.5 m), followed by NASADEM, SRTM, CEM, ASTER GDEM3 and ASTER GDEM 2, with MAE values of 3.1, 3.8, 4.6, 6.0 and 7.2 m respectively. The previously mentioned values vary according to slope and slope orientation (i.e. aspect): for flat areas (slope$\leq 5^\circ$), the NASADEM exhibits the lowest MAE (with MAE values of 1.6 for slope$\leq 1^\circ$ and

*Corresponding author
Email address: jaime-carrera@geociencias.unam.mx (J. J. Carrera-Hernández)

MAE=2.0 m when 1°<slope≤5°), whereas $MAE_{AW3D30V3}$=1.9 and 2.2 m for the previously mentioned slopes. With the use of radial boxplots developed on slope groups of 5°, it was found that both MAE and bias are increasingly affected by aspect as slope increases on all the DSMs. In the case of both AW3D30 DSMs, on flat terrain a difference of only 0.1 m in bias (i.e. median of differences with respect to LiDAR) is found between SE and NW slopes; however, this difference increases according to slope: 0.6 m for 5°<slope≤10°, 1.2 m for 10°<slope≤15°, and 1.9 m for 15°<slope≤20°. Through the analyses undertaken, it is shown that slope—and not vegetation cover—is the factor that has the largest impact on the error of DSMs, and that the effect of aspect on error increases as terrain steepens. This work shows that all DSMs present errors and that an adequate accuracy assessment of DSMs needs to consider the spatial distribution of GCPs, Difference of DSMs (DoDs) and derivatives of DSMs (i.e., slope and aspect) as the use of DoDs provide information on DSM errors (i.e. interpolation artefacts) that can not be assessed through the use of geodetic benchmarks and because DSM errors depend on both slope and aspect.

Keywords: SRTM, ASTER GDEM, AW3D30, NASADEM, LiDAR, Digital Elevation Model, Mexico.

---

1. Introduction

Topography plays a key role in climate and hydrological processes, it controls gravity driven overland and groundwater flow, it is one of the soil forming factors and has a direct impact on vegetation type (Florinsky, 2017), while hills and mountains have a direct effect on pollutant transport, weather and climate (Emeis and Knoche, 2009). The digital representation of topography—commonly referred to as Digital Elevation Model (DEM)—can be classified as either a Digital Terrain Model (DTM) or a Digital Surface Model (DSM) depending on whether it represents the bare ground (DTM) or if it also includes vegetation or man-made structures (DSM). The digital representation of terrain is the basic input used in geomorphometry (Pike et al., 2009) and spatially distributed hydrological models (Grayson and Blöschl, 2001). Accordingly, DSMs and

DTMs have been used to generate global hydrography datasets (HydroSHEDS, Lehner et al. (2008)), to identify tsunami inundation zones (Griffin et al., 2015), to develop groundwater flow models (López-Alvis et al., 2019; Westerhoff et al., 2018; Carrera-Hernández et al., 2016) and as an auxiliary variable to interpolate climatological variables (Carrera-Hernández and Gaskin, 2007). In Mexico, DEMs have been used to evaluate the presence of the Dengue Virus mosquito vector (Moreno-Madriñán et al., 2014), to predict the distribution of single-leaf pinyon in Baja California (Escobar-Flores et al., 2018), to determine the length and topography of active faults (Mendoza-Ponce et al., 2018; Lacan et al., 2018), to estimate groundwater recharge (Carrera-Hernández and Gaskin, 2008a), and for lahar hazard assessments on four different volcanoes: *Citlaltépetl* (5,600 m a.s.l., Hubbard et al. (2007)), *Popocatépetl* (5,400 m a.s.l., Huggel et al. (2008); Muñoz-salinas et al. (2009)), *Iztaccíhuatl* (5,200 m a.s.l., Schneider et al. (2008)) and *Volcán de Colima* (3,960 m a.s.l., Capra et al. (2011)).

Different global Digital Surface Models—as they do not represent the bare ground—at 30 m resolution are currently available at no cost: 1) The Shuttle Radar Topography Mission (SRTM) DSM, which was the first freely available high resolution DSM with near global coverage, 2) the Advanced Spaceborne Thermal Emission and Reflection Radiometer DSM (ASTER GDEM), and 3) the Panchromatic Remote-sensing Instrument for Stereo Mapping (PRISM) onboard the Advanced Land Observing Satellite (ALOS) DSM, from which the ALOS AW3D30 was obtained. The SRTM DSM was developed from Synthetic Aperture Radar Interferometry (InSAR, Farr et al. (2007)), while the ASTER GDEM and AW3D30 DSMs were obtained from stereophotogrammetry. The recent NASADEM—released in February 2020 (Buckley et al., 2020)—was developed by reprocessing the original SRTM data.

All DSMs are a numerical representation of the terrain and they may contain spurious artefacts and unfilled voids (Hirt, 2018). A DSM is the end result of a number of modelling and processing steps (Fisher and Tate, 2006), and it can present blunders as well as systematic and random errors (Wise, 2000). Blunders are vertical errors associated with the data collection process, while systematic errors are the result of the procedures or systems used to generate the DSM; accordingly, they follow fixed patterns that can cause bias or artefacts. These globally-available DSMs are gridded and are thus not adaptive to the terrain they attempt to represent, as they simplify the terrain's elevation on a regular spacing; this simplification results in oversampling in low-relief areas and an undersampling in high-relief areas (Wise, 2000). Because all DSMs are subject to errors, it has been recommended to assess their quality before using them (Wise, 2000); however this assessment is seldom undertaken, because users of DSMs are generally unaware of the implications and impact of DSM uncertainty on their analysis (Wechsler, 2003); as a consequence, this uncertainty is not considered when the results obtained from a DSM analysis are reported.

The accuracy of both the SRTM and GDEM DSMs has been analyzed on a global scale due to their global coverage: Berry et al. (2007) found that differences between satellite radar altimeter elevations and SRTM varied by continent, Satge et al. (2016) assessed the accuracy of the ASTER GDEM V2 using ICESat/GLAS data, while Carabajal and Boy (2016) evaluated the accuracy of the ASTER GDEM V3 dataset using ICESat laser altimetry in Greenland and Antarctica. Due to their scope, the results of the aforementioned studies are too broad and different authors have addressed the accuracy of globally available DSMs—GDEM and/or SRTM—in different countries: in the Conterminous United States (Shortridge and Messina, 2011; Gesch et al., 2016), Canada (Bolkas et al., 2016), China (Li et al., 2013, 2015), Japan (Hayakawa et al., 2008), Greenland (Hvidegaard et al., 2012), Australia (Hirt et al., 2010; Rexer and Hirt, 2014), Greece (Ioannidis et al., 2014), Croatia (Varga and Bašić, 2015), Africa (Chirico et al., 2012) and the Himalayas (Mukul et al., 2017). The only global validation study of the ALOS AW3D30 is the one developed by its validation team (Takaku et al., 2016) and similarly to the assessments of both ASTER GDEM and SRTM, its results are too broad—which is why the accuracy of the AW3D30 has been evaluated in Taiwan (Liu et al., 2015), Mindanao (Santillan and Makinano-Santillan, 2017), and Brazil (Grohmann, 2018).

Despite their wide use and that all DEMs are subject to errors (Fisher and Tate, 2006), not a single accuracy assesment has been done for neither the SRTM, ASTER

GDEM, AW3D30 or the new NASADEM DSMs in Mexico. This study aims to bridge that gap by assessing—locally and nationally—the accuracy of the previously mentioned DSMs in addition to Mexico's high resolution topography (5 m resolution) and Continous Elevation Model—both developed and distributed by Mexico's Institute of Geography and Statistics (INEGI).

2. Methodology

A total of eight Digital Surface Models (DSMs) were used in this comparison, along with land cover information derived from the 2010 Land Cover of North America developed by the North American Land Change Monitoring System collaborative initiative (NALCMS, 2020) and 83,100 geodetic benchmarks distributed throughout the country. These data were processed in the GRASS Geographic Information System (GRASS Development Team, 2020; Neteler et al., 2012) together with the R statistical software (R Core Team, 2020), with all vector atribute data stored and managed in a PostgreSQL database, according to the workflow presented in Carrera-Hernández and Gaskin (2008b). This workflow allows the use of external libraries in R such as `rgrass7` (Bivand et al., 2019), `RPostgreSQL` (Conway et al., 2017), `hydroGOF` (Zambrano-Bigiarini, 2017) and `ggplot2` (Wickham, 2016). Through this setup it is possible to analyze the large datasets compared in this work (356×10^6 cells) and to create not only visual comparisons between LiDAR and the other seven DSMs, but also to develop hexagonal-bin scatterplots (Carr et al., 1987), histograms and radial boxplots in order to identify data dispersion and localized errors.

2.1. Study Area

The use of Mexico as a case study for comparison of world-wide available DSMs is unique because it has the Pacific Ocean and the Gulf of Mexico on its Western and Eastern shores, it has two mountain ranges with abrupt elevation differences that are nearly parallel to its shores (with peaks above 5,000 m a.s.l.), and vegetation that varies according to the country's arid to tropical regions (Figure 1).

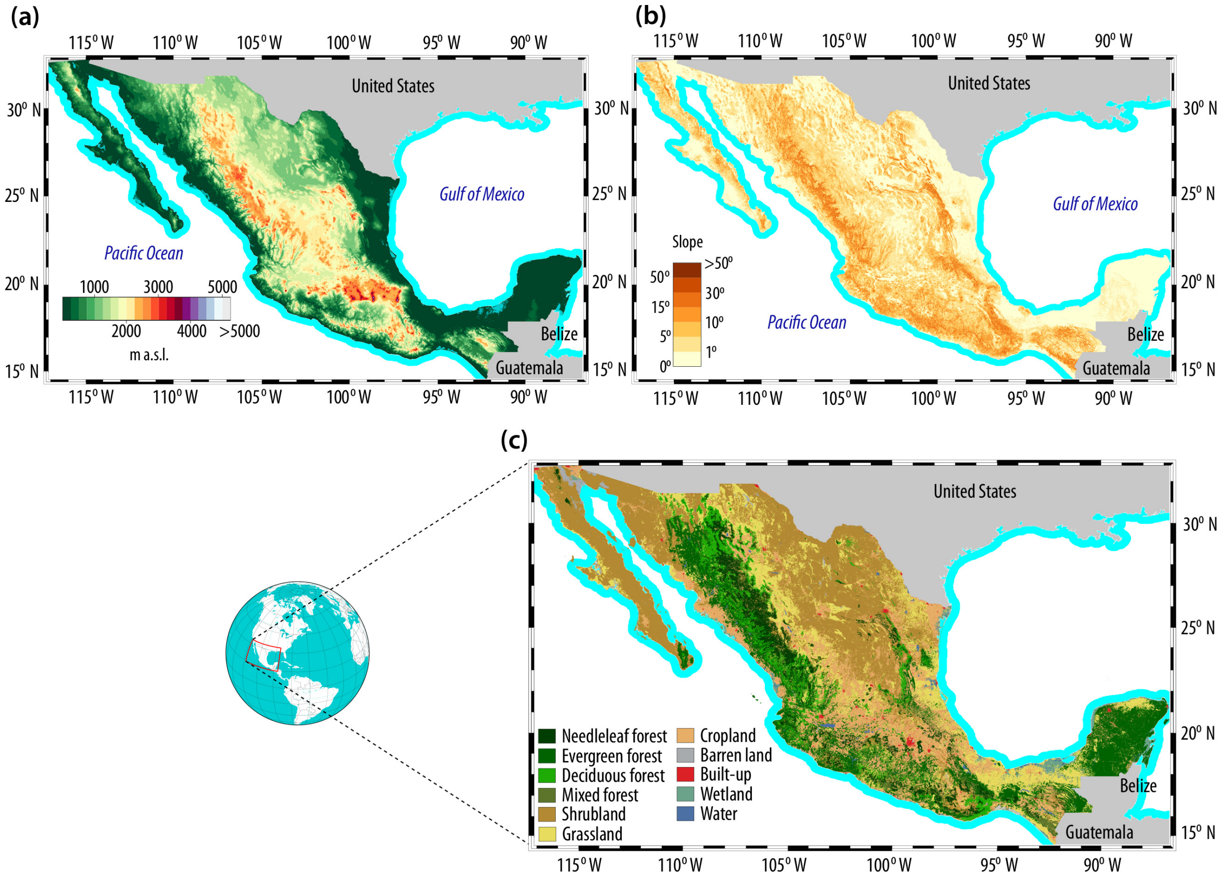

Figure 1: Physical characteristics of Mexico: (a) Topography, (b) Slope, and (c) Land Use Cover, where it can be seen that Mexico's elevations vary from 0 to 5,000 m a.s.l., with vegetation that varies from shrublands to forests. The AW3D30 V3 was used to represent both topography and slope, while Land Use Cover was regrouped from the 2010 Land Cover of North America developed by the North American Land Change Monitoring System collaborative initiative (NALCMS, 2020).

2.2. Data sets

The analyses undertaken in this work use eight DSMs available for Mexico: six of these DSMs are available for the entire world at a resolution of 30 m—ALOS AW3D30 (v2 and v3), ASTER GDEM (v2 and v3), as well as SRTM and NASADEM—another data set is available for all of Mexico at a resolution of both 15 and 30 m (Mexico's Continuous Elevation dataset, CEM), while the last DSM is available at a resolution of 5 m for some parts of Mexico (LiDAR and Satellite derived topography). These analyses are two-fold: 1) a nation-wide analysis using geodetic benchmarks distributed throughout the country, and 2) an analysis using LiDAR as reference elevation. It should be mentioned that the vertical datum varies between the datasets used: the world wide available datasets are referenced to the Earth Gravimetric Model 96 (EGM96), the CEM is referenced to the U.S. National Geodetic Vertical Datum of 1929 (NGVD29), and the high resolution topography (both LiDAR and satellite-derived) is referenced to the North American Vertical Datum of 1988 (NGVD). Both the CEM and the high resolution topography available in Mexico were referenced to the EGM96 datum using the previously developed vertical transformation grids for Mexico (Carrera-Hernández, 2020a,b).

2.2.1. *Geodetic Benchmarks*

The benchmark data were downloaded from INEGI's passive geodetic network webpage. The information for each benchmark is provided as a PDF file which has to be downloaded and processed, and a total of 83,100 PDF files were downloaded from INEGI's webpage and processed through two scripts in order to extract the required information: one script used the command line utility `pdftotext` to extract text from the PDF and another one used `awk` to process the extracted information. The PDF files used in this work correspond to INEGI's horizontal geodetic network, which is based on static measurements taken with a dual-frequency GPS/GNSS for a minimum duration of three hours—thus providing ellipsoidal heights—and adjusted to Mexico's Active Geodesic Network (RGNA, INEGI (2015)). From the inital 83,100 PDF files that were downloaded, a total of 80,584 benchmarks were used in this work after processing and cleaning the aforementioned files. As can be seen on Figure 2, these geodetic benchmarks are distributed throughout Mexico.

All of the extracted text files were grouped into one file and imported into the PostgreSQL relational database, from which a GRASS vector file was created, with its associated table stored in PostgreSQL—which can be queried and analyzed in R as described in Carrera-Hernández and Gaskin (2008b). This vector file was used to query all of the DSMs compared in this work at the location of each benchmark through the `v.what.rast` GRASS command, while the results of the query were stored on the at-

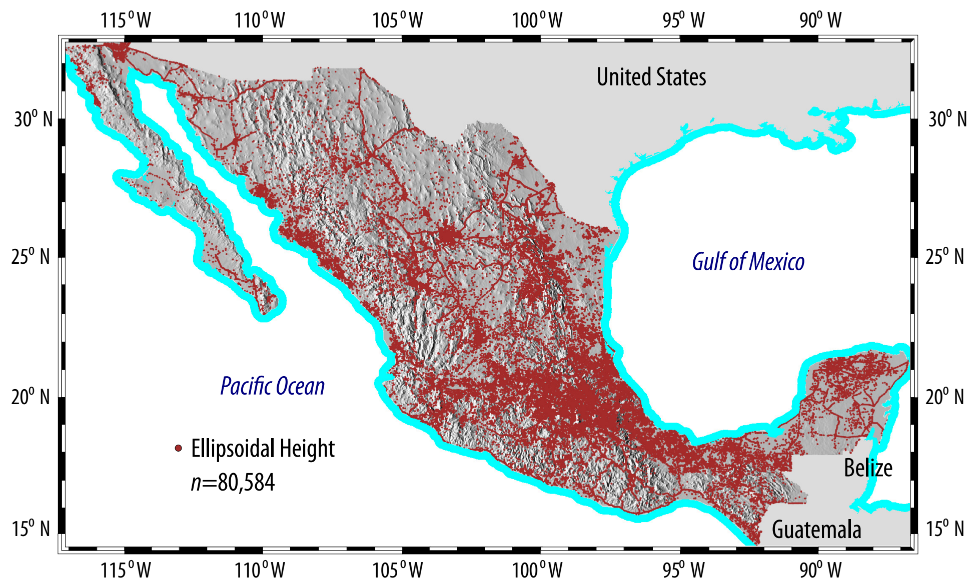

Figure 2: Spatial distribution of Mexico's horizontal geodetic network, where static measurements for a minimum duration of three hours with a dual-frequency GPS/GNSS were acquired, thus providing ellipsoidal heights that need to be converted to orthometric heights (H_{EGM96}) through the use of the EGM96 geoid height—which is the reference geoid used by the satellite derived Digital Surface Models.

tribute table associated to the vector file.

2.2.2. *High resolution topography*

Mexico's Institute of Statistics, Geography and Informatics (INEGI) distributes high resolution topography at a resolution of 5 metres for some parts of the country. This high resolution topography covers approximately 800,000 km^2 and was originally developed by LiDAR using a Leica ALS40 and processed with Terra Modeler between 2007–2011, covering an area of 370,200 km^2. After 2011, the development of high resolution topography by INEGI was done by stereophotogrammetry of Worldview imagery and currently it covers a total of 429,823 km^2.

This high resolution topography is provided by INEGI on tiles at a 1:10,000 scale that can be downloaded from INEGI's LiDAR distribution webpage, with each tile covering an approximate area of 44 km^2. Accordingly, a total of 18,082 tiles were downloaded from the aforementioned webpage—with 8,414 tiles corresponding to LiDAR derived topography and the reminder 9,668 tiles for satellite derived topography (herein referred to as HRsat). Each tile is provided by INEGI on UTM coordinates—

Mexico covers five UTM regions (11–16)—with heights referenced to the North American Vertical Datum of 1988 (NAVD88). The downloaded tiles were imported and mosaicked in each UTM zone, after which they were reprojected to geographic coordinates. Both datasets were resampled from their original resolution (5 m≈0.16666 arc sec) to 1 arc sec—in order to match the spatial resolution of the global DSMs—and through map algebra, their vertical datum was shifted with the use of Mexico's vertical datum transformation surfaces (Carrera-Hernández, 2020a,b). The areal coverage of these two datasets is shown in Figure 3, where it can be seen that although the HRsat topography covers a larger area than the LiDAR topography, its coverage is more disperse than the LiDAR topography. The metadata of both LiDAR and HRsat only mentions that geodetic benchmarks were used to reference the topography, but no information regarding its accuracy is given. Accordingly, this work presents the first vertical accuracy assessment of these two datasets.

2.2.3. CEM

The CEM data set is the *Contínuo de Elevaciones Mexicano* (Continuous Elevation data for Mexico, CEM) version 3 developed by INEGI in 2013. This DSM can be downloaded for all of Mexico at a resolution of either 15 or 30 metres and is referenced to the the U.S. National Geodetic Vertical Datum of 1929 (NGVD29, Carrera-Hernández (2020a)). The CEM is an interpolated DSM created from contour lines at a 1:50,000 scale and for its interpolation Mexico's geodetic benchmarks and water bodies were considered—although it is not specified which geodetic benchmarks were used. The interpolation of this DSM was undertaken with ANUDEM (Hutchinson, 2011), which is a discretised thin-plate spline technique where the fitted DSM is allowed to follow abrupt changes in the land surface such as streams and ridges (Hengl and Evans, 2009), allowing the enforcement of drainage conditions. With this procedure a hydrologically correct DSM is created; however, it has been found that this correction differentially compromises terrain analysis such as aspect, slope or wetness index (Callow et al., 2007).

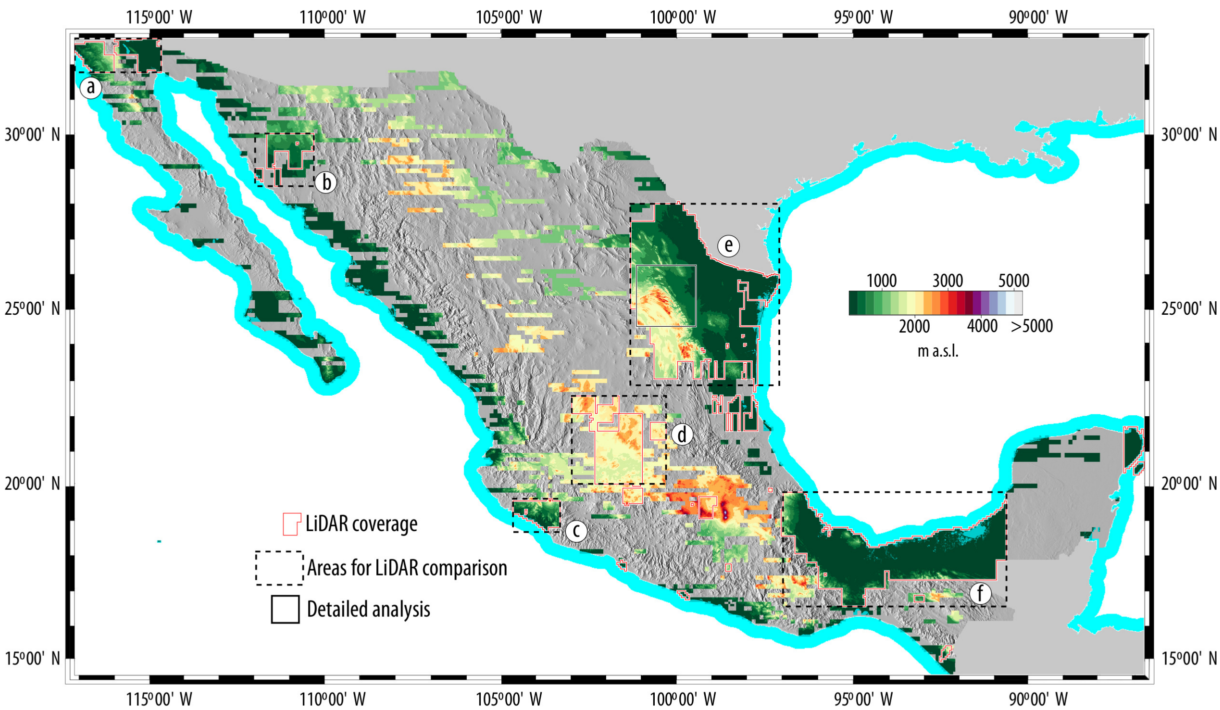

Figure 3: Areas covered by high resolution topography (5 m resolution). Enclosed red areas represent topography derived by LiDAR, while the reminder were developed by stereophotogrammetry of high resolution satellite imagery. It can be seen that although the LiDAR derived topography has lower areal coverage (370,200 km^2) than the HR satellite data (429,823 km^2), the areal coverage of LiDAR is more continuous—as the areal coverage of HRsat is more disperse. The enclosed areas in dashed lines represent the areas used for comparison of all DSMs with LiDAR data: a) Ensenada, b) Sonora, c) Colima, d) Guanajuato, e) Monterrey, and f) Tabasco.

According to its metadata, $RMSE_{CEM}$=4.8 m, which varies as a function of slope: 4.5 m on slopes between 0–14%, 6.0 m on slopes between 15–36% and 7.2 m on steeper slopes. For this work, the one-arc resolution CEM—available in geographic coordinates—was downloaded from INEGI's webpage and imported in GRASS, where its vertical datum was transformed from the NGVD29 vertical datum to the Earth Gravimetric Model 96 (EGM96) through the use of the Vertical datum transformation surfaces for Mexico (Carrera-Hernández, 2020a), available at figshare (Carrera-Hernández, 2020b).

2.2.4. *ALOS AW3D30*

This Digital Surface Model was developed by Japan's Aerospace Exploration Agency (JAXA) from the archived data of the Panchromatic Remote-sensing Instrument for Stereo Mapping (PRISM) onboard the Advanced Land Observing Satellite (ALOS), which was launched on January 24th, 2006. The details of the instruments and their corresponding calibration are given in Takaku et al. (2007) and Tadono et al. (2008). The PRISM was an optical sensor designed to generate worldwide data and operated from 2006 to 2011; originally a 5 m resolution DSM—the Advanced World 3D DSM (AW3D)—was generated, with both vertical and horizontal RMSE values of 5 meters (Takaku et al., 2016). To generate the DSM, the stereo images were processed in units of 35$\times$35 km and then mosaicked onto $1^\circ \times 1^\circ$ tiles (Takaku et al., 2014); this processing was finished world-wide in March 2016. The original DSM at 5 m resolution is commercially available, while a 30 m DSM derived from the original—the AW3D30 DSM—is freely available and distributed on $1^\circ \times 1^\circ$ tiles.

The validation of the AW3D was undertaken by using ICEsat and LiDAR data along with GCPs in different parts of the world (Takaku et al., 2016). The LiDAR comparison was undertaken on a 52$\times$57 km tile (2,964 km^2) with a resolution of 2.5 meters, and 4,628 GCPs from which difference statistics were obtained, with minimum and maximum differences of $\pm$30 meters; however, 70% of these GCPs (3,247) were located in Japan and only 27 GCPs in Mexico. The ALOS AW3D30 was developed by obtaining the mean of a 7$\times$7 cell moving window of the original AW3D data (Tadono et al., 2016), with its validation undertaken through the use of 5,121 GCPs for 127 tiles—most of them located in Japan—with a resulting RMSE=4.4 m and a SD=4.38 m (Tadono et al., 2016).

The AW3D30 V1.1 was released in March 2017, followed in April 2018 by V2.1, on which offset errors from the ICESat reference were corrected; a year later, V2.2 was released, on which both missing and "cloud and snow" pixels were filled with data from other DSMs. The latest version—AW3D30 V3.1, which used new supplementary data for void filling and alteration of coastline data—was released in April 2020. The vertical accuracy of the last two AW3D30 versions (V2.2 and V3.1)—which can be downloaded from the ALOS webpage—is determined in this work.

2.2.5. ASTER GDEM

The first version of the ASTER GDEM—released in June 2009 as a research grade product (Slater et al., 2011)—was generated using over 1.2 million images collected by the ASTER instrument onboard Terra and was generated using the ASTER stereo image archive from 2000 to August 2008 (Urai et al., 2012). The improved GDEM V2—released in 2011—included 260,000 additional images acquired from September 2008 to August 2010 (Urai et al., 2012), improving coverage and reducing the occurrence of artefacts. The ASTER GDEM2 accuracy assessments included three different comparisons (Tachikawa et al., 2011): 1) geodetic references over the Conterminous United States, 2) national elevation grids over both the US and Japan and, 3) SRTM data set over the U.S. and 20 sites located in Afghanistan, Argentina, Australia, Bolivia, Bosnia, Canada, China, Iraq, Kazakhstan, Korea, Libya, Nigeria, Phillipines, Russia, Thailand and Alaska (Slater et al., 2011). A comparison of the ASTER GDEM2 with ICESat altimetry is summarized for Africa, Australia, Eurasia, North America, South America, New Zealand, Western Europe and Greenland in Tachikawa et al. (2011). The minimum and maximum elevation differences between the GDEM2 and ICESat data for South America were of -376.38 and 1,242.94 m respectively, while for North America these differences were of -514.4 and 2,761.3 metres. For North America, the reported RMSE=11.92 m, while for South America the RMSE=8.78 metres (Tachikawa et al., 2011).

The third version of the ASTER GDEM (GDEM3, Abrams et al. (2020)) was released on August 2019, and compared to GDEM2, this latest version has a decrease in elevation void area due to the increase of ASTER stereo image data and improved software processesing. Due to the recent release of GDEM3, only a handful of analyses on its verticual accuracy have been developed: using ICESat data, Carabajal and Boy (2016) found that GDEM3 displays smaller means, similar medians and less scatter than GDEM2 in both Greenland and Antarctica. For the Conterminous United States, Gesch et al. (2016) used 23,115 points of the "GPS on benchmarks" dataset of geodetic control points from the U.S. National Geodetic Survey. With these GPS points, the aforementioned authors report that $RMSE_{GDEM3}$=8.52 m with a mean of -1.20 m (compared to a $RMSE_{GDEM2}$=8.68 m and $RMSE_{GDEM1}$=9.34 m obtained with the same points). In this work, the accuracy of both GDEM2 and GDEM3 is assessed, even though GDEM2 has been decomissioned and is not currently available for download.

2.2.6. SRTM

The Shuttle Radar Topography Mission (SRTM) was flown onboard the space shuttle Endeavour in February 11–22 of 2000 and it employed both a C and an X band system (Farr et al., 2007). NASA's Jet Propulsion Laboratory (JPL) was responsible for the C radar, from which the global SRTM data was derived. The SRTM DSM is currently distributed by the USGS and was developed to meet absolute horizontal and vertical accuracies of 20 and 16 meters respectively and it is a Digital Surface Model because the SRTM radars were unable to sense the surface beneath vegetation canopies (Farr et al., 2007). The objective of the SRTM was to use synthetic aperture radar interferometry (InSAR) to collect sufficient data to generate a DSM of the 80% of the global landmass that lies betwenn $\pm 60°$ latitude (Buckley et al., 2020). The SRTM V3 is the latest version that can be downloaded from the USGS Earth Explorer, and for this version the previously existing voids (V2 and V1) have been filled with the GDEM2, the Global Multi-resolution Terrain Elevation Data 2010 (GMTED2010), and the National Elevation Dataset (NED; NASA (2015)). Although the one-arc data were originally only availabe to the U.S. territory, they were made available for the entire globe in 2016.

Two types of voids have been previously identified on the SRTM DSM (Shortridge and Messina, 2011): 1) large diamond-shaped coverage gaps, due to a lack of data collection during several orbits, and 2) smaller and irregularly located voids due to surface characteristics. The accuracy of this DSM was globally assessed by Rodríguez et al. (2006) through the use of kinematic GPS transects. However, the transects used to validate the SRTM data in North America were only located in Canada and the United

States, while the transects used in South America were only located in Argentina, Chile and Peru. The absolute height difference reported in that study was of 9.0 m in North America and 6.2 m in South America, and as stated by the authors, the distribution of the GCPs used was non-random, with the majority of the GCPs densely packed in a small number of geographic areas.

2.2.7. NASADEM

The NASADEM is the successor of the NASA SRTM V3 and was developed by reprocessing the original SRTM raw signal radar data by using improved algorithms and reference data derived from the Ice, Cloud and Land Elevation Satellite (ICESat)—which were unavailable during the original SRTM processing (Buckley et al., 2020). The remaining voids were primarily filled with GDEM2, GDEM3 and AWD3D30 data through the use of a modified delta surface fill method to achieve a seamless merge.

Because the NASADEM was recently released (February 2020), the number of studies that have assessed its vertical accuracy is limited. The accuracy assessment undertaken by its development team through the use of ICESat data (10×10^6 bare ground and 9×10^6 vegetated points on CONUS and southern Canada) found that $\mathrm{RMSE}_{\mathrm{NASADEM}}$=5.3 metres (Buckley et al., 2020). Through the use of 573 points, Gesch (2018) found that $\mathrm{RMSE}_{\mathrm{NASADEM}}$ =3.1 m and $\mathrm{MAE}_{\mathrm{NASADEM}}$ =2.47 metres, while Uuemaa et al. (2020) reported that $\mathrm{RMSE}_{\mathrm{NASADEM}}$ varies from 6.39 m in Estonia up to 12.08 m in New Zealand, concluding that the NASADEM only represents a slight improvement in comparison to SRTM and that DEM accuracy is a function of slope, without relationship to slope orientation.

2.3. Dataset comparison

From the previous section, it can be inferred that newer versions of the satellite derived DSMs use more data or better processing algorithms. The amount of data used on each DSM is referred to as stack number, which varies spatially according to each DSM as shown in Figure 4, where it can be seen that the maximum stack number for each DSM is different and that the remaining voids of each DSM were filled with data from other DSMs. As can be seen on Fig. 4(a), the void cells of the AW3D30 V2 DSM were filled with data from both GDEM2 and SRTM, while SRTM voids were filled with GDEM2 data (Fig. 4b). As shown in Fig. 4(c) GDEM2 does not have other DSM values, while for the AW3D30V3 data from GDEM3, GDEM2 and SRTM were used to fill in its voids (Fig. 4(d)). This Figure also shows how the new NASADEM (Fig. 4(e)) improves the stack number of the original SRTM, although a diamond shaped void area—filled in with GDEM2 as well—is still present on the north of Mexico.

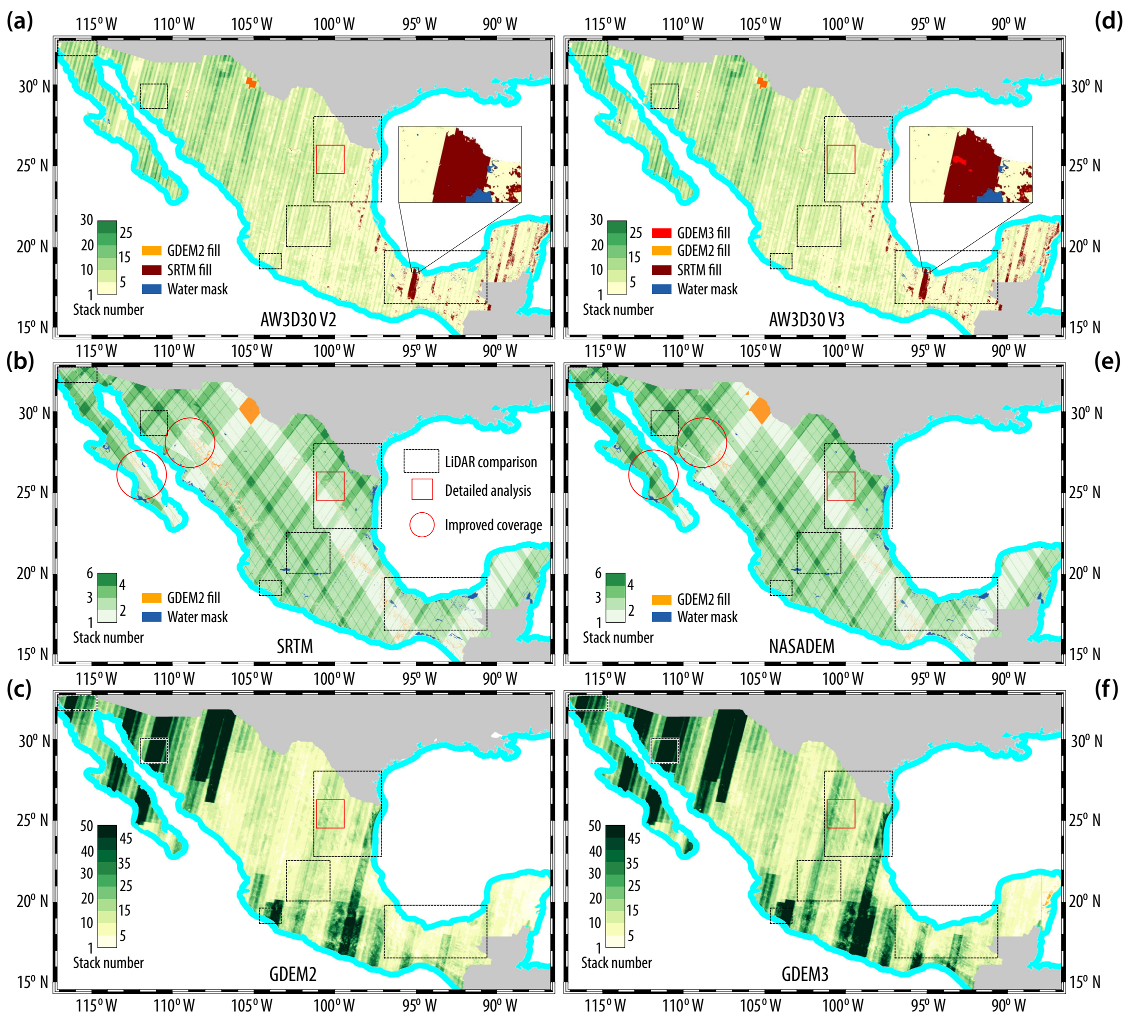

Figure 4: Stack number and auxiliary data used to fill in voids for each satellite derived Digital Surface Model: a) AW3D30 V2, b) SRTM, c) GDEM2, d) AW3D30 V3, e) NASADEM, f) GDEM3. The coverage improvement of NASADEM over SRTM and of GDEM3 over GDEM2 can be appreciated on some parts of Mexico. However, the NASADEM still exhibits the large diamond shaped coverage gaps of the SRTM in northern Mexico.

A total of 222 tiles from each satellite-derived DSM (GDEM2 and GDEM3, AW3D30 V2 and V3, SRTM and NASADEM) were downloaded from their respective distribution pages, while a total of 18,082 high-resolution topography tiles were downloaded from INEGI and processed as previously described. A two-fold approach was used in the dataset comparison: 1) nation-wide analysis using benchmark data, and 2) local analysis using LiDAR data as reference. It should be mentioned that the comparison undertaken in this work considers only elevations from each DSM, not the void-filled cells with other DSMs.

2.3.1. Statistical analysis

Gridded DSMs are representations of terrain and are thus subject to errors, which are quantified through the use of reference data. These data are normally geodetic benchmarks, from which the Root Mean Square Error (RMSE), mean error (ME), and Standard Deviation (SD) are determined. Two problems arise with the use of the RMSE as an accuracy measure: a) it is based on a small sample of checkpoints, and b) it does not assist in identifying whether the error is random, systematic or blunder (Wise, 2000). The drawbacks of using checkpoints to validate a DEM are that they should be randomly distributed, and sufficiently large in order to obtain reliable measures (Höhle and Höhle, 2009); in addition, the assumption that the errors on DEMs derived from photogrammetry follow a normal distribution does not apply due to errors caused by filtering or interpolation (Höhle and Höhle, 2009). In order to overcome the previously mentioned shortcomings of using the RMSE, ME, and SD, this work determines other metrics that have been recommended to report the accuracy of DSMs due to their robustness and distribution free approach to handle outliers: the Mean Absolute difference (MAE), the Median and the Normalized Median Absolute Deviation (NMAD; Höhle and Höhle (2009); Willmott and Matsuura (2005)).

Because the RMSE, ME and SD are accuracy measures for DEMs that are generally reported, they are also reported herein for comparison purposes. These values are estimated as:

$$RMSE = \sqrt{\frac{\sum_{i=1}^{n}(z_i - zt_i)^2}{n}} \tag{1}$$

where z_i refers to the i^{th} DEM elevation, zt_i refers to the i^{th} known or measured elevation (i.e., reference), and n is the number of measurements. The standard deviation is determined by:

$$SD = \sqrt{\frac{\sum_{i=1}^{n}\left((z_i - zt_i) - \hat{\mu}\right)^2}{n-1}} \tag{2}$$

where z_i refers to the i^{th} DEM elevation, zt_i refers to the i^{th} known or measured elevation (i.e., reference), n is the number of measurements and $\hat{\mu}$ represents the mean difference. As described by Willmott and Matsuura (2005), the RMSE varies with the variability of error magnitude, the square root of the number of differences ($n^{\frac{1}{2}}$), and the magnitude of the average difference—which turns out to be the Mean Absolute Error. Because of this, the MAE is considered unambiguous and a more natural measure of average difference (Willmott and Matsuura, 2005) and is determined by:

$$MAE = \frac{\sum_{i=1}^{n}|z_i - zt_i|}{n} \tag{3}$$

where y_i refers to the i^{th} known or measured elevation.

The Normalized Median Absolute Deviation (NMAD) represents the median of the absolute deviations from the median and is considered as an estimate for the standard deviation more resilient to outliers in the dataset (Höhle and Höhle, 2009) which is computed by:

$$NMAD = 1.4826 \times median_i(|(z_i - zt_i) - m_{\Delta h}|) \tag{4}$$

where $m_{\Delta h}$ is the median of the errors, showing that the NMAD is thus proportional to the median of the absolute difference between errors and the median error.

3. Results and discussion

3.1. Accuracy assesment using geodetic benchmarks

The accuracy of the eight DSMs available for Mexico was first analyzed by using the geodetic benchmarks as elevation reference; it should be mentioned that these benchmarks provide ellipsoidal heights, which were converted to orthometric heights using the EGM96 geoid heights, as detailed in Carrera-Hernández (2020a). Because the high resolution topography available was generated with two different methodologies—LiDAR and photogrammetry from stereoscopic high resolution satellite data (HRsat)—this dataset is divided in two. As previously mentioned, the areal coverage of LiDAR is 370,200 km^2, while that of HRsat is 429,823 km^2, although the areal coverage of HRsat is more dispersed (Figure 3). Accordingly, the analysis undertaken with the geodetic benchmarks is first done on: a) area covered by LiDAR data (n_{bench}=24,175), b) area covered by HRsat (n_{bench}=25,015), and c) national area (n_{bench}=80,584), as summarized in Figure 5. Not surprisingly, the LiDAR DSM exhibits the lowest MAE (1.96 m), while HRsat has a MAE=2.27 m and for the three areas considered, the MAE obtained for the CEM was lower than for the satellite-derived DSMs (MAE_{CEM}=2.57, 2.62 and 3.08 m for the LiDAR, HRsat and national areas respectively) and also has less dispersion (Fig. 5). However, the MAE difference between the CEM and both versions of AW3D30 is small for the three areas (between 2.6–3.0 m for the first two areas and 3.1 m for the national comparison).

The spatial distribution of the differences between each DSM and the geodetic benchmarks is shown in Figure 6, where the bias at each benchmark for each DSM can be appreciated—a positive bias occurs when the DSM is above a given benchmark, while the DSM is below the benchmark in the case of a negative bias. It can be seen that the CEM, NASADEM, GDEM3 and GDEM2 have negative bias, while both versions of the AW3D30, as well as the SRTM DSMs have positive bias (represented by the median in Fig. 5).

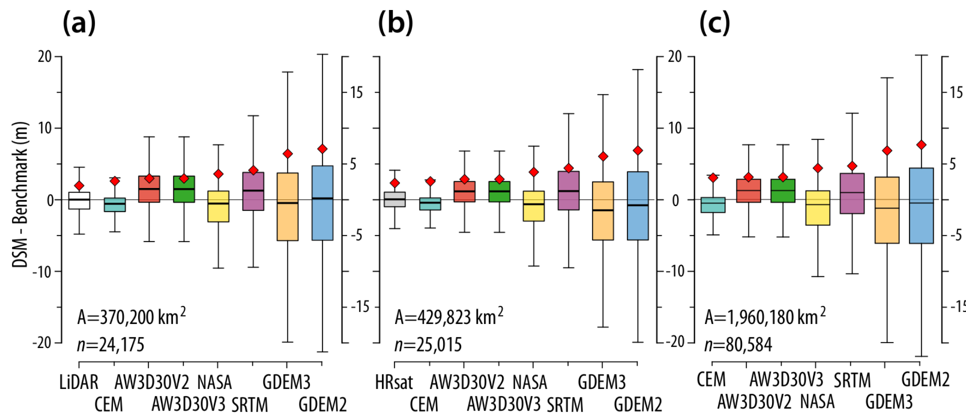

Figure 5: Errors for each of the DSM considered: (a) area covered by LiDAR data, (b) area covered by high resolution satellite data, and (c) national coverage. A negative median represents that the DSM is below the elevation of the reference data—which is also referred to as negative bias.

3.2. Comparison with LiDAR data.

Although the geodetic benchmarks used in the previous analysis are distributed throughout Mexico, a more detailed analysis —considering land cover, slope and aspect— can be undertaken using the LiDAR DSM as reference and be used to develop Difference of DEMs (DoDs), which are

The LiDAR DSM can be used as reference elevation because it has the lowest MAE value of all DSMs considered (MAE=1.96 m for all the areas covered by LiDAR). A detailed comparison of the differences of each DSM with both benchmark and LiDAR data can be seen on Figure 7, in a 34,000 km^2 area located in Mexico's northeast—as shown by the red rectangle of Fig. 4—with elevations that range from sea level up to 3,000 m (Fig. 3). As can be appreciated in Fig. 7a, this area encompasses a total of 2,417 benchmarks and nearly 38×10^6 cells (Fig. 7b). In the aforementioned figures, it can be seen that when either the geodetic benchmarks or LiDAR are used as reference elevation, all DSMs exhibit a similar MAE—except for the CEM, which has a MAE $= 2.2$ m when compared with the geodetic benchmarks, but a MAE=4.8 m when compared with LiDAR (for this area MAE$_{\text{LiDAR}}$=1.8 m). The Difference of DEMs (DoDs) between the CEM and LiDAR (Fig. 7b) shows interpolation artefacts in different regions and the carving effect caused by the enforcement of drainage conditions on the CEM. The

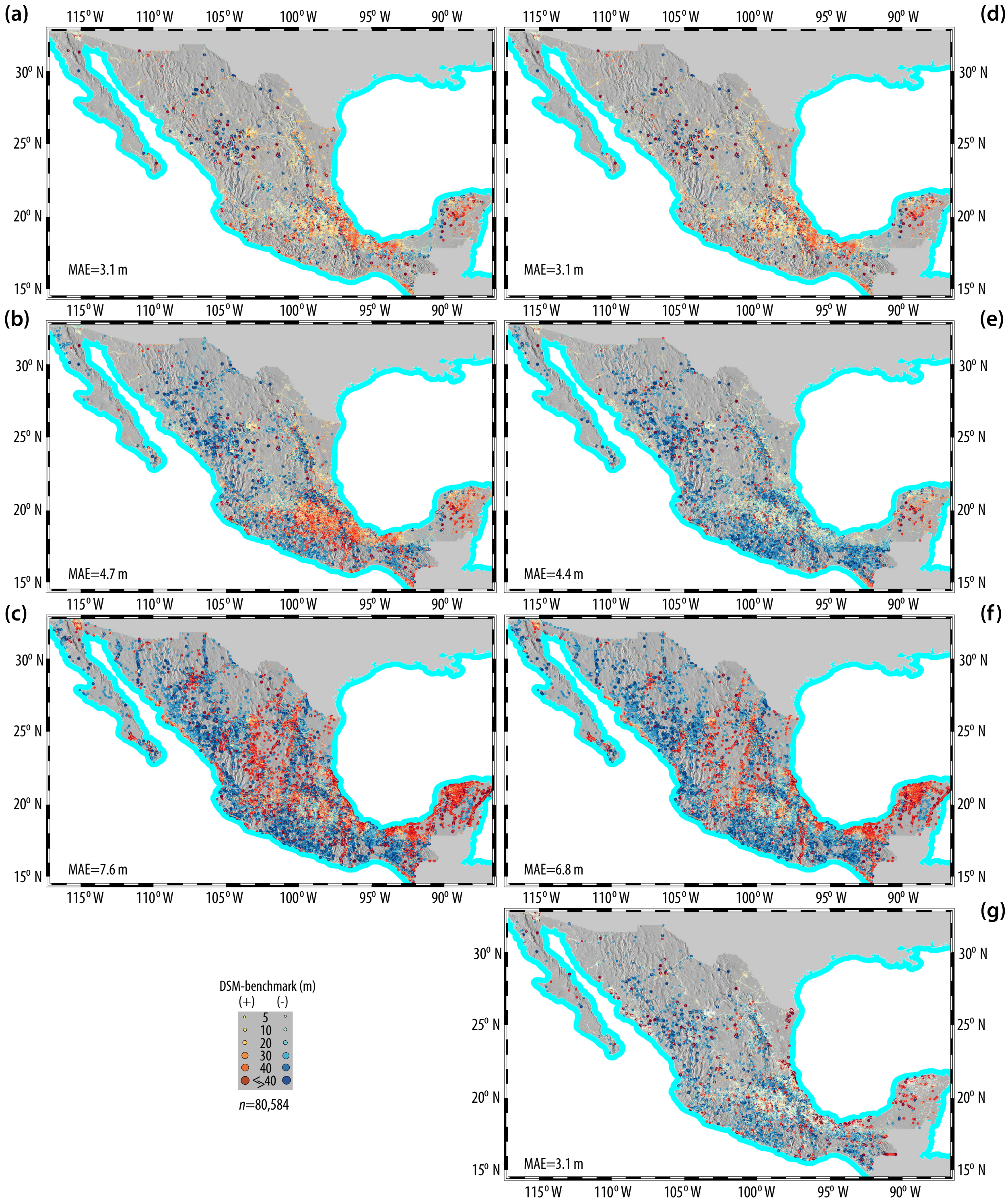

Figure 6: Differences between orthometric heights registered at the geodetic benchmarks and the seven DSMs considered: a)AW3D30 V2, b) SRTM, c) GDEM2, d) AW3D30 V3, e) NASADEM, f) GDEM3, g) CEM. Positive values occur where the DSM is above the benchmarks, while negative values appear where the DSM is below the benchmark.

DoDs shown in Fig. 7b illustrate the importance of using a reference DEM to analyze the accuracy of other DEMs in addition to geodetic benchmarks, as the measurements acquired with a GPS can not be exhaustive. With the use of a reference DEM, further analyses based on slope and slope orientation (aspect) can also be developed.

In order to have the largest number of LiDAR adjancent tiles, six different areas located in different regions of Mexico (Fig. 3) were used to compare the seven DSMs with LiDAR. A true-color composite of these areas is shown in Figure S1, where the difference in vegetation cover between them can be seen. The land cover and elevation variability of each area is shown in Figure 8, where it can be seen that shrubland, grassland and cropland represent the main land cover types for most of the considered areas (Fig. 8a).

(a) Ensenada: This region covers 18.72×10^6 cells and is located in Mexico's northwestern border with the United States, and 15% of it is barren land (Fig. 8a), with a median elevation of approximately 100 m, although its elevation range is nearly 1,750 m (Fig. 8b). Within this area is where Mexico's lowest elevation point—the Salada Lagoon (-10 m)—is found (Carrera-Hernández, 2020a).

(b) Sonora: This region covers 14.39×10^6 cells, with a median elevation of 600 m (Fig. 8(b))—although some cells are found at sea level (Fig. S1(b)). Nearly 70% of this area is covered by shrubland, with approximately 15% covered by decidious forest, while 11% of it is grassland (Fig. 8(a)).

(c) Colima: This area comprises the smallest cell count (10.25×10^6), but nearly 50% of it is covered by deciduous forest (Fig. 8(a)), with a median elevation of 550 m, but a variability of approximately 1,700 m in elevation (Fig. 8(b)). The *Volcán de Colima* is found within this area, reaching an elevation of nearly 3,960 metres.

(d) Guanajuato: This area is located in central Mexico and covers one of Mexico's main irrigated areas (Carrera-Hernandez, 2018), which can be easily identified on Fig. S1(d). This area has an elevation that varies from around 1,600 to 2,800 m

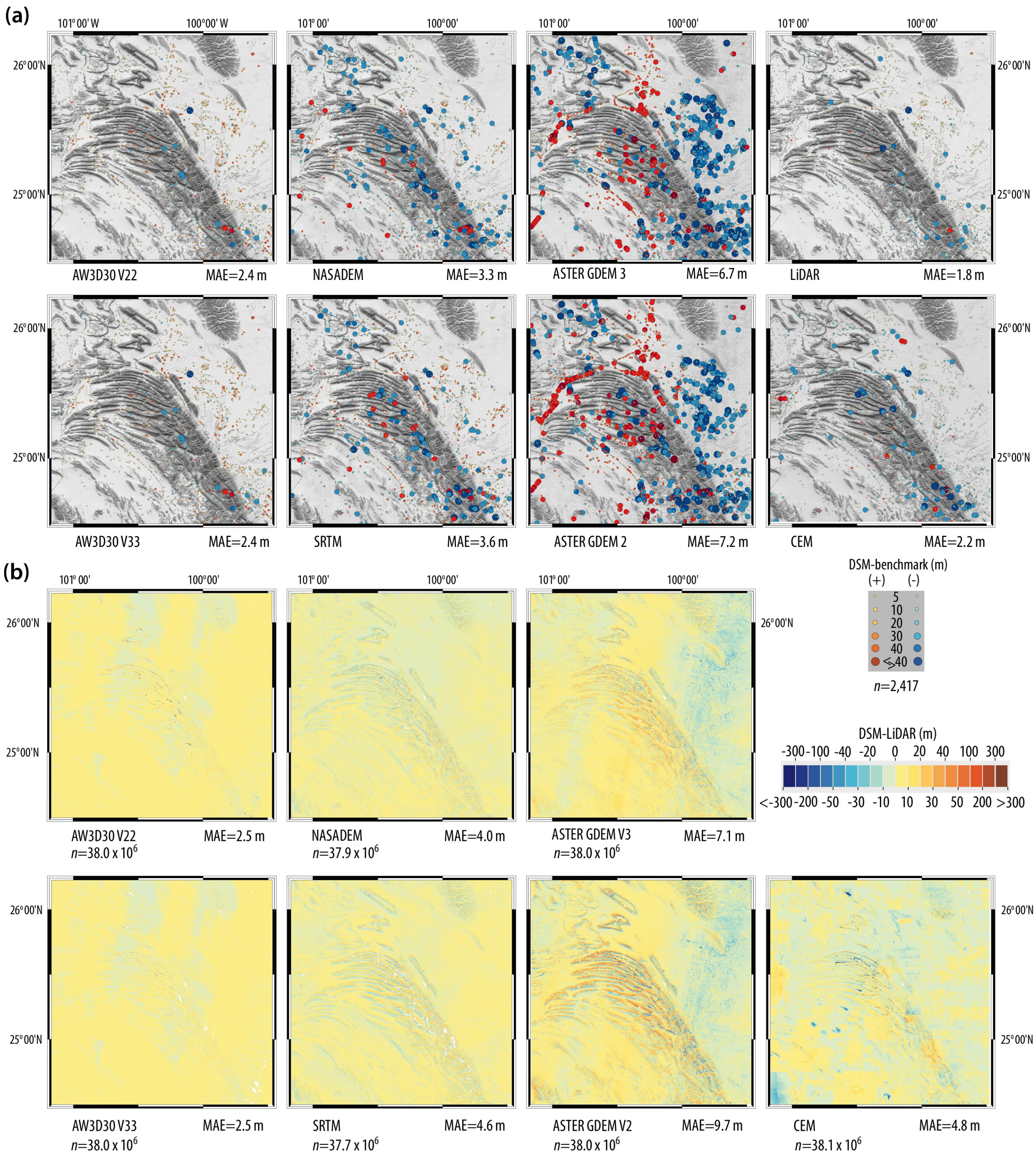

Figure 7: Differences between the Digital Surface Models considered with respect to (a) geodetic benchmarks and (b) LiDAR. The shaded reliefs were developed using multiple light sources for each DSM according to the guidelines provided by Gantenbein (2012). The number of cells of each DoD varies because only non-filled cells of each DSM were used in the comparison (Fig. 4)—filled cells with data from other DSMs are shown in white color on the DoDs.

with a median of 2,050 m (Fig. 8(b)), and 50% of the 42.74×10^6 cells that comprise it are cropland.

(e) Monterrey: This is the largest area considered (162.59×10^6 cells), and the one with the largest variability in elevation, varying from sea level up to 3,000 metres, although it has a median elevation of 400 m (Fig. 8(b)). The city of Monterrey—the third largest urban settlement in Mexico—is found within this area.

(f) Tabasco: This is the second largest area (115.74×10^6 cells) and nearly half of it (55%) is covered by grassland (Fig. 8(a)). However, 16% of this area comprises evergreen forest, located on its southern region, while other 15% is cropland.

When the six previously mentioned areas are grouped, the main land cover is grassland (30%), followed by shrubland (30%) and cropland (21%)—which add up to 80% of the total area. The remainder land cover is comprised of deciduous, evergreen and needle leaf forest (5.6%, 5.2% and 2.23% respectively), built up area (1.8%), barren land (1%) and mixed forest (0.5%). Although the percentage coverage of mixed forest is low, a total of 1.54×10^6 cells comprise this land cover, while deciduous, evergreen and needle leaf forests are represented by 20.41, 18.82 and 8.13×10^6 cells.

By comparing all the LiDAR cells covered in the aforementioned areas with the seven DSMs ($n \approx 352 \times 10^6$), the obtained differences differ from the differences observed with the Geodetic Benchmarks. As can be seen on Figure 9, both versions of the AW3D30 exhibit the same MAE (2.5 m), while both NASADEM and SRTM have lower MAE values (3.1 and 3.8 m) than the CEM (4.6 m), which contrasts to the MAE obtained when the geodetic benchmarks were used as reference data (Fig. 5; $\text{MAE}_{\text{NASADEM}} = 4.38$, $\text{MAE}_{\text{SRTM}} = 4.69$, $\text{MAE}_{\text{CEM}} = 3.08$ m). When LiDAR is used as reference data, the dispersion of the CEM is also larger than the dispersion of both AW3D30 versions, NASADEM and SRTM (Fig. 9).

The MAE values shown in Figure 9 do not give information on whether the error varies by slope, by slope orientation or by land cover. Using LiDAR as reference data,

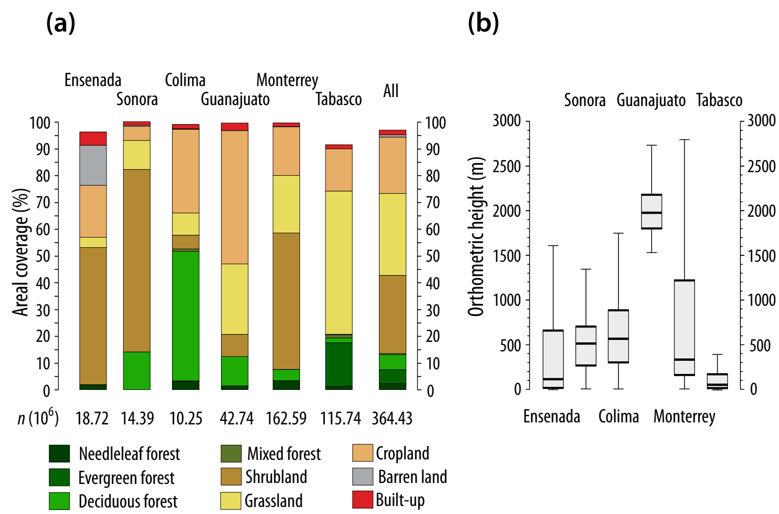

Figure 8: Summary of (a) Land Cover and (b) Elevation for the six areas used to compare LiDAR with the seven DSMs. The location of each area is shown in Fig. 3. The areal coverage of some areas do not add up to 100% because other land cover types (i.e., wetlands and water) were not considered in these analyses.

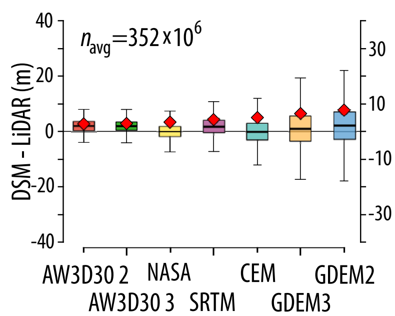

Figure 9: Differences between LiDAR and the seven DSMs considered. The number of cells used varies according to the DSM considered due to the fact that only cells with values of each DSM were used in the analysis (i.e., void cells filled with values from other DSMs were not considered): n_{CEM}=356.4$\times 10^6$ while $n_{\mathrm{AW3D30\ V3}}$=342.4$\times 10^6$ cells.

the aforementioned information can be obtained, as summarized in Figure 10 and detailed in Table 1 for slopes≤45°. The slope-grouped boxplots of Fig. 10 show how the MAE increases as slope increases and how MAE varies according to slope orientation (aspect). This information is enriched with both a bias scatterplot and histogram—for which the frequency of bias was determined at every 0.2 meters. The results of Fig. 10 show that the MAE increases with slope, but also varies according to aspect.

For both AW3D30 versions, the variation of MAE according to aspect is of approximately 0.6 m (2.2 on SE slopes compared to 2.8 on NW slopes as shown in Fig. 10a and d); however, this difference increases on the other satellite derived DSMs as the MAE difference is of nearly 1.3 for SRTM when aspect is considered (3.2 on SE slopes and 4.5 on NNW and N slopes, Fig. 10b). It should be noted that the aspect derived MAE of the NASADEM is different than that of the SRTM, as the NASADEM MAE forms an ellipse with its largest axis oriented on the NW-SE direction (with a maximum difference of approximately 0.7 m when compared to the NE-SW facing slopes). The variation of MAE with respect to slope orientation also occurs when GDEM2 and GDEM3 are compared, as the ellipse formed by the aspect-derived MAE for GDEM2 (with its major axis also oriented in the NW-SE direction) changes to a circle on the GDEM3 (Fig. 10c, f).

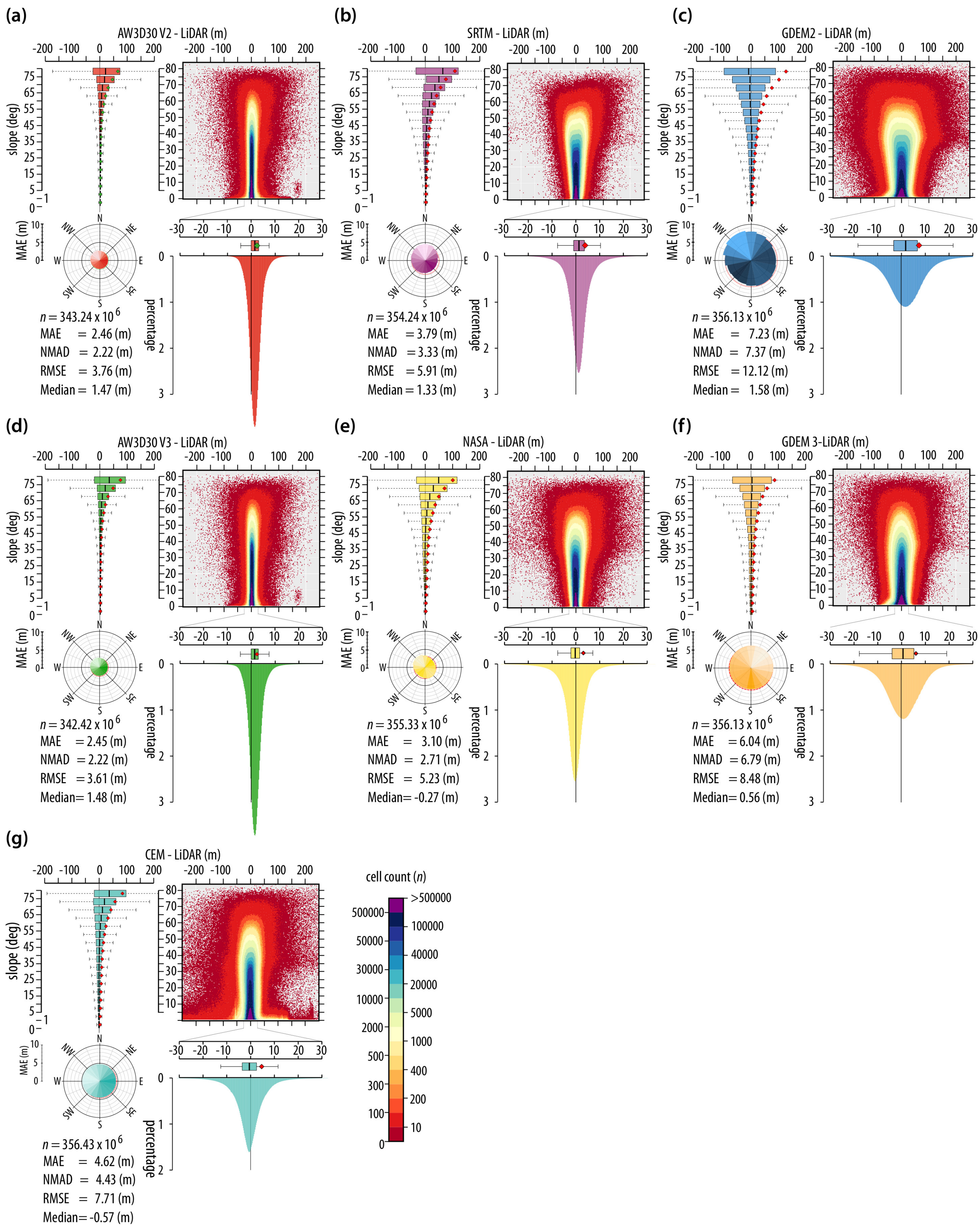

Figure 10: Differences (i.e., bias) between the seven Digital Surface Models considered with respect to LiDAR. The differences are shown as hex-bin scattergrams and histograms (with intervals of 0.2 m) and grouped according to slope and aspect for each DSM: (a) AW3D30 V2, (b) SRTM, (c) GDEM2, (d) AW3D30 V3, (e) NASA, (f) GDEM3, and (g) CEM.

Table 1: Summary statistics of all DSMs according to slope variation.

		Slope (degrees)										
		All	0-1	1-5	5-10	10-15	15-20	20-25	25-30	30-35	35-40	40-45
MAE (m)	AW3D30 2	2.5	2.0	2.2	2.5	2.8	3.1	3.4	3.7	4.2	4.8	6.0
	AW3D30 3	2.5	1.9	2.2	2.5	2.8	3.1	3.4	3.7	4.1	4.8	5.9
	NASADEM	3.1	1.6	2.0	3.3	4.6	5.8	6.8	7.9	9.1	10.8	13.1
	SRTM	3.8	2.3	2.7	3.9	5.2	6.4	7.6	9.0	10.7	12.8	15.5
	CEM	4.6	3.2	3.8	5.0	5.9	6.7	7.5	8.4	9.6	11.0	13.1
	GDEM 3	6.0	5.2	5.1	6.0	7.0	7.8	8.7	9.6	10.8	12.5	14.6
	GDEM 2	7.2	5.3	5.5	7.0	8.7	10.4	12.3	14.6	17.7	21.2	24.8
Median (m)	AW3D30 2	1.5	1.2	1.5	1.7	1.8	1.9	1.9	2.1	2.1	2.3	2.6
	AW3D30 3	1.5	1.2	1.5	1.7	1.8	1.9	1.9	2.1	2.1	2.3	2.6
	NASADEM	-0.3	-0.3	-0.2	-0.3	-0.6	-0.9	-1.2	-1.3	-1.1	-0.6	0.0
	SRTM	1.3	1.0	1.5	1.7	1.8	1.7	1.8	1.9	2.2	3.1	4.4
	CEM	-0.6	-0.4	-0.7	-0.6	-0.5	-0.5	-0.7	-0.8	-0.6	0.1	0.8
	GDEM 3	0.6	1.0	0.2	0.1	0.2	0.4	0.6	1.0	1.6	2.0	1.5
	GDEM 2	1.6	1.9	1.3	1.2	1.2	1.4	1.6	2.1	2.7	3.1	1.8
NMAD (m)	AW3D30 2	2.2	1.9	2.0	2.3	2.6	3.0	3.4	3.8	4.4	5.1	6.3
	AW3D30 3	2.2	1.9	2.0	2.3	2.6	3.0	3.3	3.8	4.4	5.1	6.3
	NASADEM	2.7	1.8	2.3	3.7	5.5	7.1	8.6	10.0	11.6	13.3	15.5
	SRTM	3.3	2.7	3.2	4.5	6.1	7.7	9.5	11.6	14.1	16.8	19.9
	CEM	4.4	3.2	4.1	5.5	6.4	7.5	8.6	10.0	11.5	13.2	15.6
	GDEM 3	6.8	6.3	6.0	7.0	8.1	9.1	10.1	11.2	12.6	14.4	16.6
	GDEM 2	7.4	6.3	6.5	8.3	10.4	12.5	14.9	18.0	21.9	26.2	30.2
RMSE	AW3D30 2	3.8	2.8	3.0	3.5	4.0	4.4	4.8	5.6	6.3	7.6	9.5
	AW3D30 3	3.6	2.7	2.9	3.4	3.9	4.3	4.8	5.4	6.1	7.1	8.9
	NASADEM	5.2	2.2	2.8	4.4	6.1	7.4	8.7	10.1	11.8	14.2	17.9
	SRTM	5.9	2.9	3.6	5.2	6.8	8.2	9.6	11.3	13.3	16.0	19.7
	CEM	7.7	5.6	6.3	7.6	8.6	9.5	10.6	11.6	13.1	15.2	18.5
	GDEM 3	8.5	6.7	6.7	7.9	9.2	10.4	11.5	12.7	14.4	16.8	19.8
	GDEM 2	12.1	7.0	7.3	9.3	11.6	14.1	17.2	21.4	26.1	32.8	41.2
Mean	AW3D30 2	1.6	1.2	1.5	1.7	2.0	2.1	2.2	2.4	2.5	2.7	3.1
	AW3D30 3	1.6	1.2	1.5	1.7	2.0	2.1	2.2	2.4	2.4	2.6	3.1
	NASADEM	-0.3	-0.2	-0.2	-0.3	-0.5	-0.7	-0.9	-1.0	-0.8	-0.2	0.8
	SRTM	1.5	1.0	1.5	1.9	2.0	2.0	2.0	2.0	2.2	2.9	4.2
	CEM	-0.6	-0.3	-0.7	-0.8	-0.6	-0.6	-0.9	-1.0	-0.8	-0.1	0.6
	GDEM 3	0.4	0.9	0.0	-0.2	-0.1	0.0	0.2	0.7	1.5	2.1	1.7
	GDEM 2	1.5	1.8	1.1	1.0	1.2	1.5	1.9	2.4	3.1	3.6	2.5
SD	AW3D30 2	3.4	2.5	2.5	3.0	3.5	3.8	4.3	5.0	5.8	7.1	8.9
	AW3D30 3	3.2	2.4	2.5	3.0	3.4	3.8	4.2	4.9	5.5	6.6	8.4
	NASADEM	5.2	2.2	2.8	4.4	6.1	7.4	8.7	10.0	11.7	14.2	17.9
	SRTM	5.7	2.8	3.3	4.8	6.5	8.0	9.4	11.1	13.1	15.7	19.2
	CEM	7.7	5.6	6.2	7.6	8.6	9.5	10.5	11.5	13.1	15.2	18.5
	GDEM 3	8.4	6.6	6.7	7.9	9.2	10.4	11.5	12.7	14.4	16.7	19.7
	GDEM 2	12.0	6.7	7.2	9.2	11.5	14.0	17.1	21.3	25.9	32.6	41.1
ncells (10^6)	AW3D30 2	343.24	115.24	118.25	36.23	20.15	15.49	12.73	10.17	7.52	4.38	1.79
	AW3D30 3	342.43	114.96	118.00	36.17	20.13	15.47	12.71	10.15	7.50	4.35	1.77
	NASADEM	355.34	117.49	122.11	38.66	21.45	16.40	13.42	10.64	7.76	4.44	1.78
	SRTM	354.24	117.45	122.02	38.56	21.38	16.34	13.36	10.56	7.64	4.29	1.67
	CEM	356.43	117.74	122.15	38.67	21.46	16.42	13.47	10.74	7.91	4.60	1.90
	GDEM 3	356.01	117.65	122.07	38.65	21.44	16.40	13.45	10.72	7.88	4.57	1.88
	GDEM 2	356.14	117.72	122.10	38.64	21.43	16.40	13.45	10.71	7.89	4.58	1.89
	avg	351.97	116.89	120.96	37.94	21.06	16.13	13.23	10.53	7.73	4.46	1.81

In addition to the slope-derived boxplots that summarize the bias of each DSM, Fig. 10 also shows a hex-bin scattergram for each DSM, where the bias dispersion can be appreciated. The dispersion of negative bias on flat areas for both GDEM versions can be seen on their respective scattergrams (Fig. 10c,f) as well as for the CEM (Fig. 10g). This is better appreciated on Table 1, where it can also be seen that when slope$\leq$5° the NASADEM provides the smallest MAE (1.6 m for slope$\leq$1° and 2.0 m when 1°<slope$\leq$5°) and even the lowest NMAD (1.8 m) when slope$\leq$1°. This represents a 30% improvement when slope$\leq$1° and 25% when 1°<slope$\leq$5° even though

this improvement is of 18% when all slopes are considered ($MAE_{NASADEM}$=3.1 m, MAE_{SRTM}=3.8 m, as detailed on Table 1). This improvement constrasts with that of the GDEM3 over GDEM2 (which improved its MAE from 7.2 to 6.0 m when all slopes are considered) because this improvement is more significant when slope$\geq$5° than on flat terrain (Fig. 10c, f and Table 1).

These results show that the bias of all DSMs depends on slope but do not provide any information on whether or not bias varies according to land cover—a question that is addressed in the following section.

3.2.1. Land cover-based slope analysis

To analyze how the difference between LiDAR and the other DSMs varies according to both slope and land cover, the 2010 Land Cover of North America developed by the North American Land Change Monitoring System collaborative initiative (NALCMS, 2020) was regrouped in 11 categories (Fig. 1). Excluding both water and wetlands from the regrouped version, a total of 63 hex-bin scattergrams of differences for each DSM with respect to LiDAR were determined in order to show how elevation differences are related to slope for each land cover type. The 63 hex-bin scatterplots obtained (Figure 11), show how the bias of each DSM varies according to both slope and land cover—a variation that can not be appreciated when a boxplot is used to summarize the respective bias of each case (which is also shown at the bottom of each hex-bin scatterplot). The aforementioned scatterplots show how both AW3D30 versions have the same dispersion for all cover types (Fig. 11a,b—which are in agreement with the summary statistics shown in Table 1), that the CEM exhibits dispersion on flat areas for shrubland, grassland and cropland (Fig. 11e), that the GDEM3 (Fig. 11f) has less dispersion than the GDEM2 for all land cover types (Fig. 11g) and that the GDEM2 has the largest bias dispersion of all the DSMs considered. This Figure also shows that the four types of forest areas exhibit the largest MAE for all DSMs.

To provide a better insight into the effect that both land cover and slope have on bias, the scattergrams of Fig. 11 were processed into slope-grouped boxplots at every

5°, except for flat areas (slope≤5°), which were divided in two groups: 1) slope≤1°, and 2) 1°<slope≤5°. The resulting boxplots are shown in Figure 12, where it can be appreciated that the MAE, bias (i.e. median), and interquartile range increase according to slope—although this relationship is different for each DSM. In the case of AW3D30 V2 and V3, NASADEM, SRTM and CEM the bias tends to be positive (i.e. the DSM is above LiDAR) and increase as slope increases for all the types of land cover considered. This is also the case for both GDEM versions when areas covered by forest (needleleaf, evergreen, deciduous and mixed) are analised; however, the absolute value of negative bias increases for shrubland, grassland, cropland, barren land and built-up areas as terrain steepens.

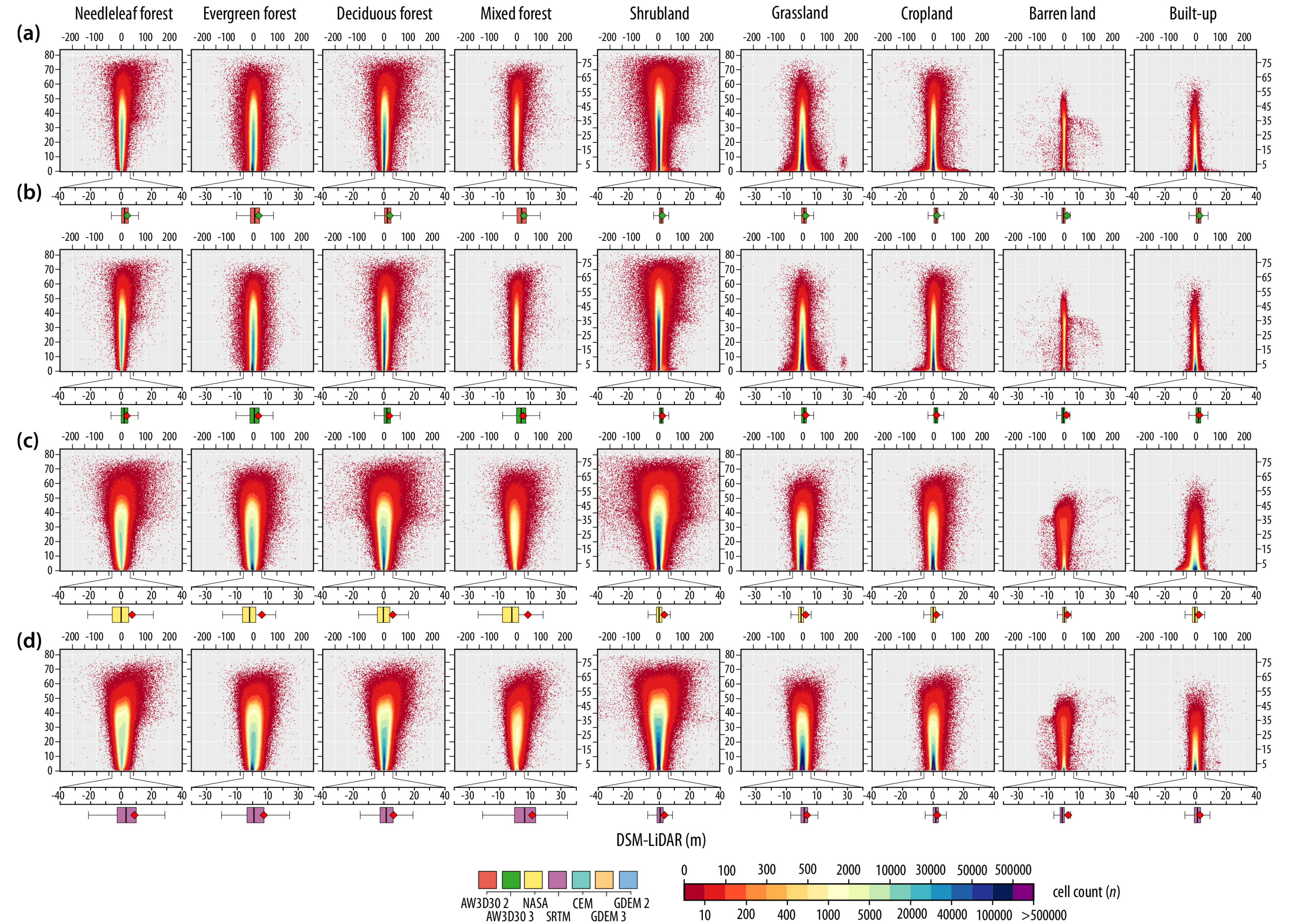

Figure 11: Hex-bin scattergram and boxplots of bias according to land cover type and DSM: (a) AW3D30 V2, (b) AW3D30 V3, (c) NASADEM, (d) SRTM, (e) CEM, (f) GDEM3, (g) GDEM2. Note the scale change for the boxplots shown at the bottom of each scattergram.

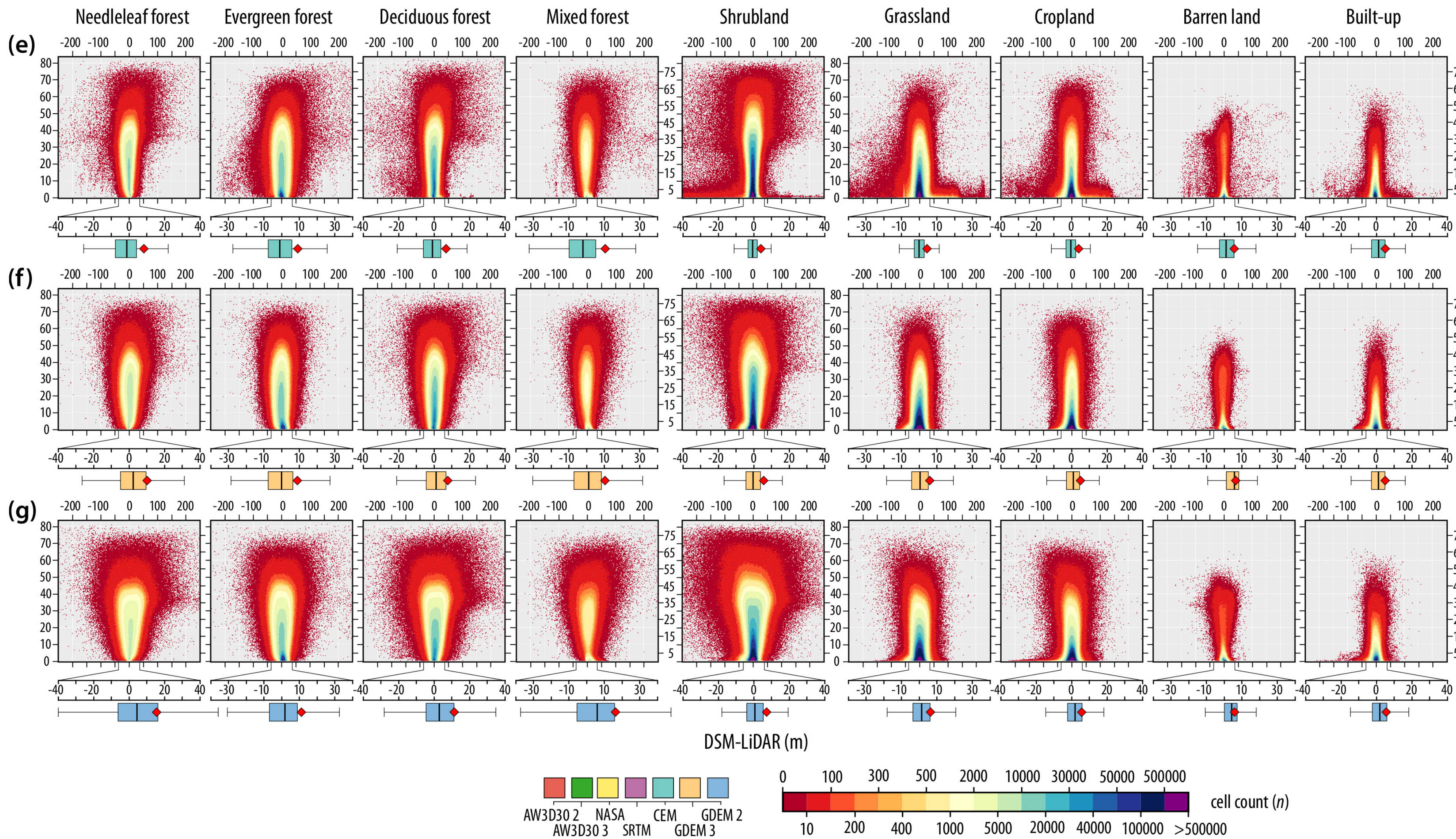

Figure 11 (Cont.): Hex-bin scattergrams of bias according to land cover type and DSM: (a) AW3D30 V2, (b) AW3D30 V3, (c) NASADEM, (d) SRTM, (e) CEM, (f) GDEM3, (g) GDEM2. Note the scale change for the boxplots shown at the bottom of each scattergram.

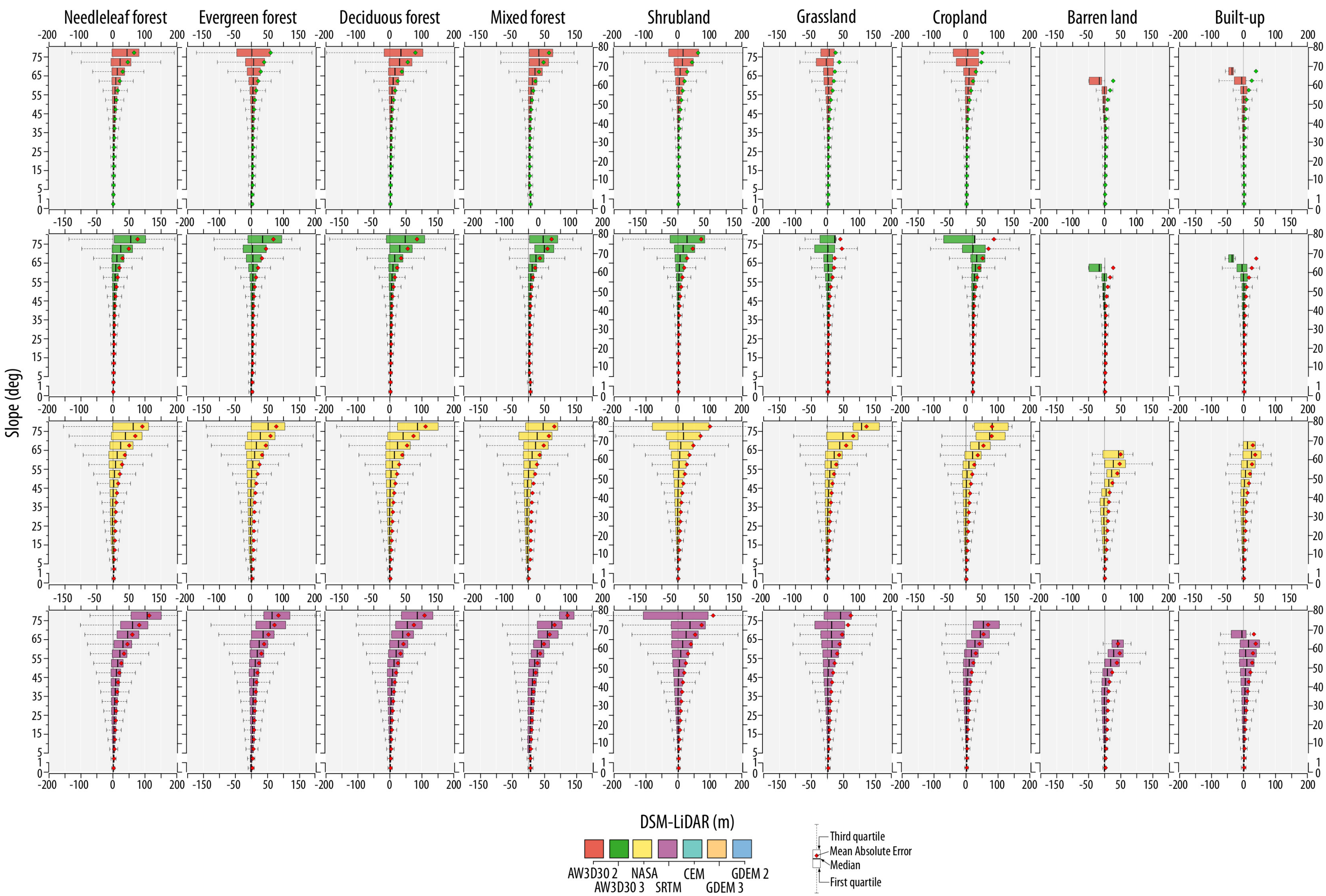

Figure 12: Slope-grouped boxplots of bias according to land cover type and DSM: (a) AW3D30 V2, (b) AW3D30 V3, (c) NASADEM, (d) SRTM, (e) CEM, (f) GDEM3, (g) GDEM2.

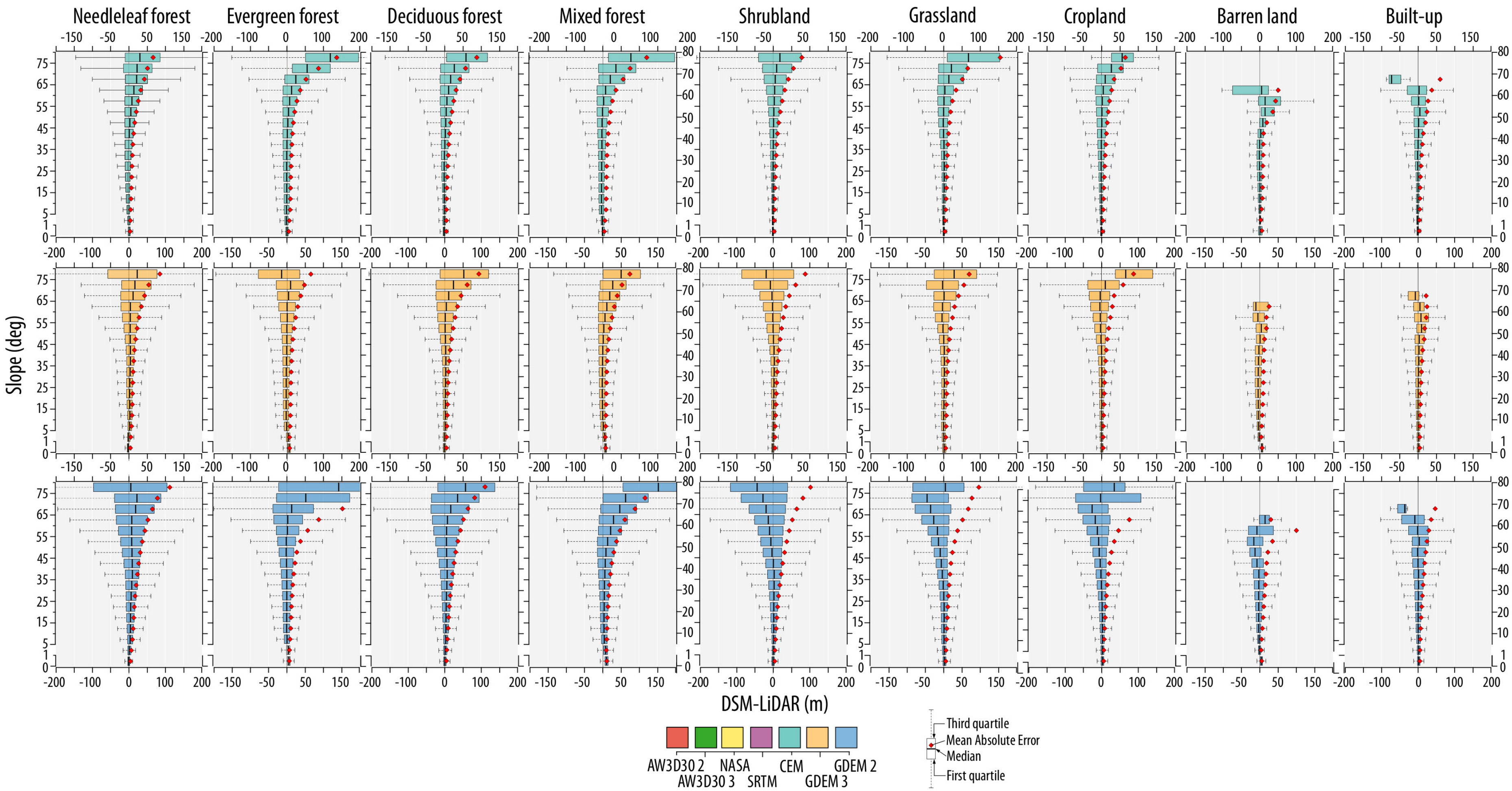

Figure 12 (Cont.): Slope-grouped boxplots of bias according to land cover type and DSM: (a) AW3D30 V2, (b) AW3D30 V3, (c) NASADEM, (d) SRTM, (e) CEM, (f) GDEM3, (g) GDEM2.

3.2.2. *Land cover-based aspect analysis*

Because the MAE of each DSM varies according to aspect (Fig. 10), a further analysis based on both aspect and land cover is undertaken. For this analysis, the MAE of each land cover type was determined for the seven DSMs considered at 16 slope orientations (i.e. aspect), along with the global MAE for each case as shown in Figure 13, where it can be seen that the largest MAE is obtained on forest-covered areas and that MAE varies according to aspect. This figure shows that all DSMs tend to have larger MAE values on both NW and NNW facing slopes while the contrary occurs on SE facing slopes, except on the NASADEM for the needleleaf forest covered areas (Fig. 13). From this Figure, it could be inferred that MAE varies according to cover type, and that the large MAE found in areas covered by needle leaf and mixed forest is caused by vegetation. However, by overlaying the spatial distribution of forested areas with slope (Fig. 1b and c), it can be seen that these cover types are found on both flat and steep terrain, as is clearly shown in Figure 14. The results of Figs. 13 and 14 show that slope—and not vegetation cover—is the main factor that controlls the Mean Absolute Error (MAE). To clarify this situation a slope-based aspect analysis is required, which is detailed in the following section.

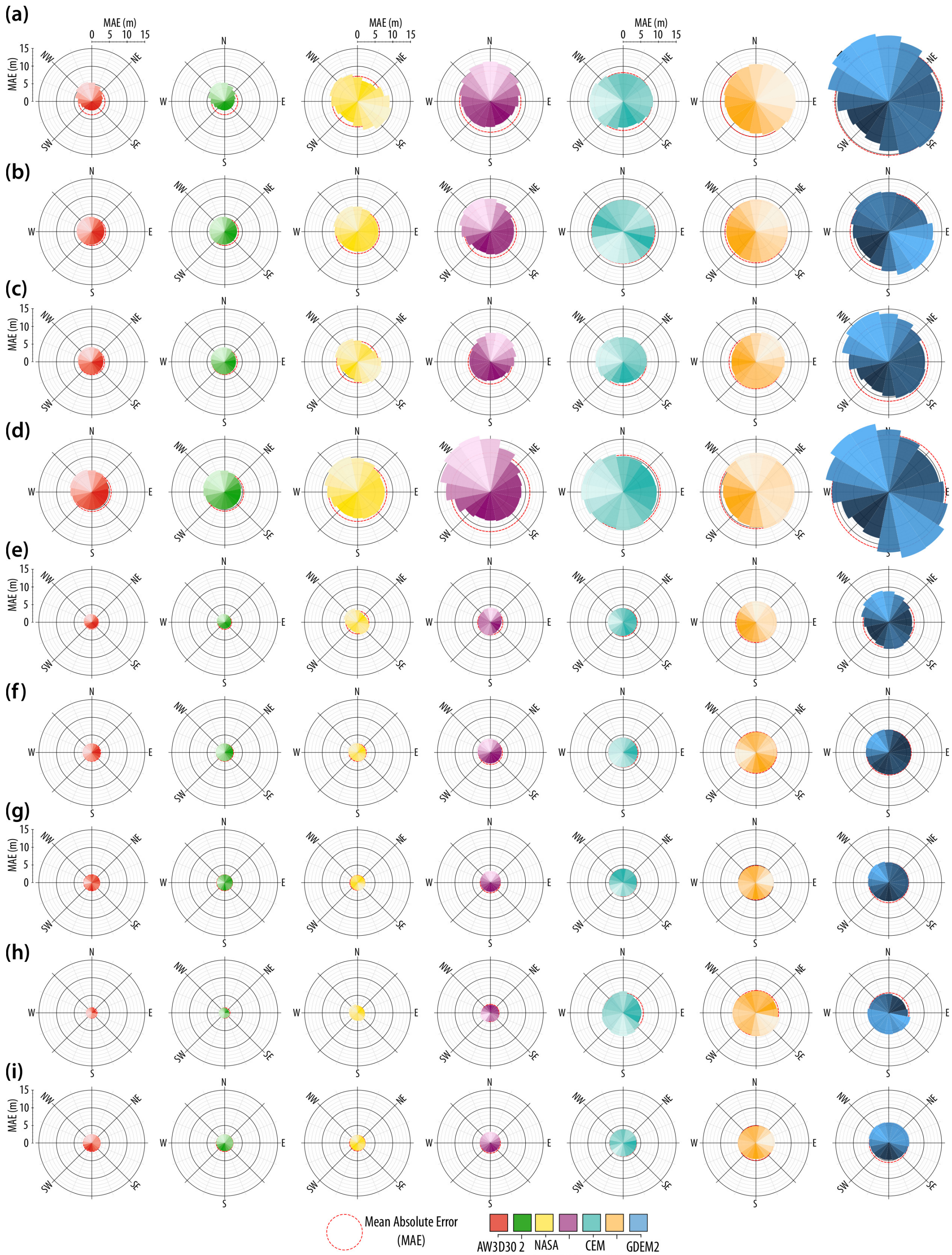

Figure 13: Land cover-based aspect analysis of the Mean Absolute Error (MAE) obtained by comparing seven Digital Surface Models to LiDAR.

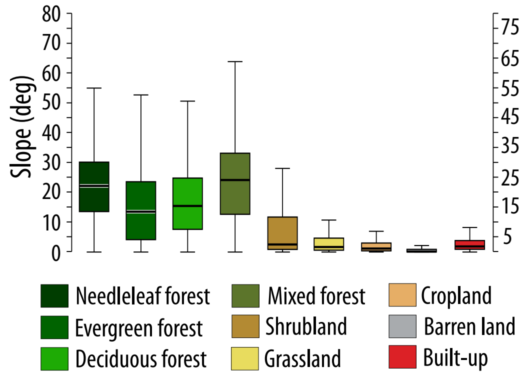

Figure 14: Land cover and its relationship to slope.

3.2.3. *Slope-based aspect analysis*

A question that still needs to be addressed is whether or not the bias of each DSM varies according to the slope orientation for each of the slope groups that have been considered. The previous section showed that slope is the main factor that affects bias; however—as can be seen on Fig. 13—bias varies according to aspect as a function of land cover. The aforementioned Figure shows that the land cover type that exhibits the largest variation of bias as a function of aspect is mixed forest, which is found on both flat and steep areas (Fig. 14), just as the other forest types—which exhibit the largest variation of MAE according to aspect. To improve the previously undertaken analyses, this section focuses on how bias changes according to both slope and aspect by first grouping biases in blocks of increasing slope—as done in the land cover and slope section—and then by analysing the bias in each slope orientation (16 in total, as done in Fig. 14). In this manner, it was possible to develop radial boxplots that show how the MAE varies according to aspect in each slope group along with the first, second and third quartiles. These radial boxplots (Fig. 15) show how both the MAE and bias are increasingly affected by aspect as slope increases—even for both versions of AW3D30—as detailed on Tables S1 and S2.

As can be seen on Fig. 15, both versions of AW3D30 increase their positive bias toward the NW as slope increases, while the same occurs for negative bias on the SE direction, thus the circle formed by the radial boxplot of these two DSMs on flat terrain "shifts" and increases its interquartile range toward the NW—a shift that increases according to slope (Fig. 15a–j). This shifting occurs on all the DSMs considered, although their shifting direction and magnitude varies for each DSM. Of interest are the different shifting modes between the NASADEM and the SRTM, as the radial boxplot of the latter shifts northward as slope increases, while for the former this shift occurs toward the SE (Fig. 15); as detailed in Tables S3 and S4, the NASADEM—which is the result of reprocessing the original SRTM data—represents an improvement over SRTM V3, particularly on flat terrain, where it even provides a better vertical accuracy than the AW3D30 DSM.

By comparing the radial boxplots of both GDEM versions (Fig. 15), it can be seen that GDEM3 improved the vertical accuracy of GDEM2, as the aspect-based interquartile range shift caused by slope increase observed on GDEM2 is diminished on GDEM3. The latest GDEM version does not exhibit the large negative/positive bias of GDEM2 on SE/NW facing slopes (-3.97 and 7.11 m respectively when $10^{\circ} < \text{slope} \leq 15^{\circ}$, compared to -0.49 and 1.17 m for the same aspect and slope on GDEM3, as can be seen on Tables S6 and S7). However, despite the vertical accuracy improvement of GDEM3, it still has larger MAE values and more dispersion than AW3D30 and NASADEM.

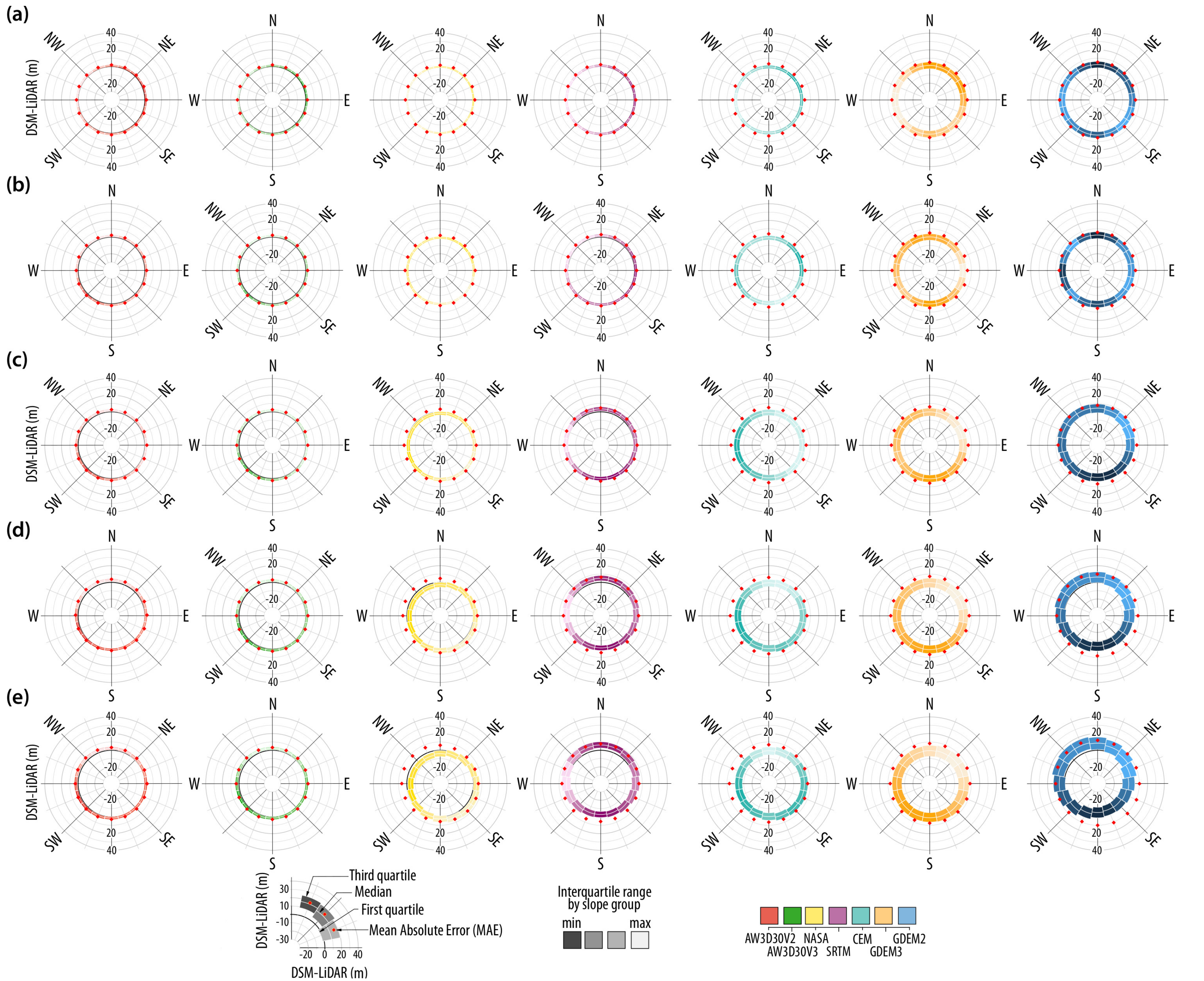

Figure 15: Radial boxplots between the seven DSMs considered and LiDAR according to aspect grouped by slope: (a) slope$\leq 1°$, (b) $1° <$slope$\leq 5°$, (c) $5° <$slope$\leq 10°$, (d) $10° <$slope$\leq 15°$, (e) $15° <$slope$\leq 20°$, (f) $20° <$slope$\leq 25°$, (g) $25° <$slope$\leq 30°$, (h) $30° <$slope$\leq 35°$, (i) $35° <$slope$\leq 40°$, (j) $40° <$slope$\leq 45°$

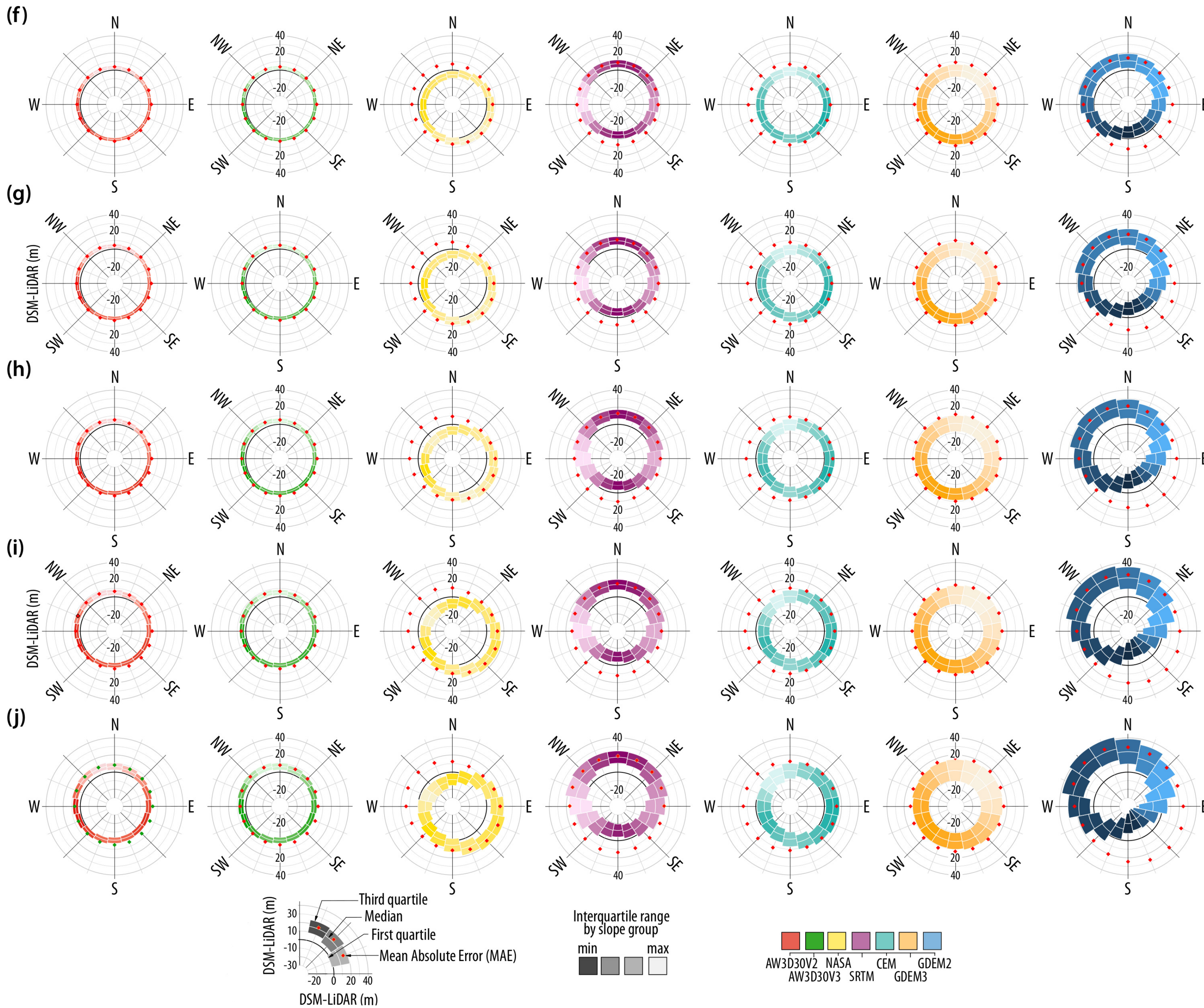

Figure 15 (Cont.): Radial boxplots between the seven DSMs considered and LiDAR according to aspect grouped by slope: (a) slope≤ 1°, (b) 1°<slope≤ 5°, (c) 5°<slope≤ 10°, (d) 10°<slope≤ 15°, (e) 15°<slope≤ 20°, (f) 20°<slope≤ 25°, (g) 25°<slope≤ 30°, (h) 30°<slope≤ 35°, (i) 35°<slope≤ 40°, (j) 40°<slope≤ 45°

4. Conclusions and recommendations

This work presents the first accuracy assessment of eight different Digital Surface Models—ALOS AW3D30 V2 and V3, GDEM2, GDEM3, SRTM, NASADEM, LiDAR and Mexico's Continuous Elevation Model (CEM)—in Mexico. Using geodetic benchmarks as reference elevation on those areas covered by LiDAR (A_{LiDAR}=370,200 km^2, n_{bench}=24,175), it was found that LiDAR has the best vertical accuracy of all DSMs considered ($\text{MAE}_{\text{LiDAR}}=1.96$ m, $\text{MAE}_{\text{CEM}}=2.57$ m, $\text{MAE}_{\text{AW3D30}}=2.99$ m, $\text{MAE}_{\text{NASADEM}}=3.58$ m, $\text{MAE}_{\text{SRTM}}=4.13$ m, $\text{MAE}_{\text{GDEM3}}=6.79$ m, $\text{MAE}_{\text{GDEM2}}=7.64$ m).

Using the LiDAR DSM as reference elevation, seven Difference of DEMs (DODs) were developed with the remainder DSMs in order to undertake analyses based on both slope and slope orientation (aspect) as well as land cover. For the aforementioned analyses, an average of 351×10^6 cells were used, resulting in $\text{MAE}_{\text{AW3D30V2}}=\text{MAE}_{\text{AW3D30V3}}=2.5$ m, $\text{MAE}_{\text{NASADEM}}=3.1$ m, $\text{MAE}_{\text{SRTMV3}}=3.8$ m, $\text{MAE}_{\text{CEM}}=4.6$ m, $\text{MAE}_{\text{GDEM3}}=6.0$ m, and $\text{MAE}_{\text{GDEM2}}=7.2$ metres. However, it was also found that MAE is a function of both slope and aspect, and that the bias found on different vegetation types is caused by the aforementioned variables and not by vegetation cover—as the areas covered by forest (which exhibit the largest MAE values) are found on both flat and steep terrain. The variation of elevation difference according to both slope and aspect was analyzed by first grouping the differences between LiDAR and the other seven DSMs in blocks of increasing slope and then by analysing the difference in each of the 16 aspects considered through the development of radial boxplots, which clearly show how both the MAE and bias are increasingly affected by aspect as slope increases, even for both versions of AW3D30.

The NASADEM represents an improvement over SRTM V3, particularly on flat terrain, where it even provides a better vertical accuracy than the AW3D30 DSM, as it was found that on flat terrain (slope$\leq5^\circ$), the NASADEM provides the lowest MAE value—even better than that obtained with the AW3D30 DSM ($\text{MAE}_{\text{NASADEM}}=1.6$ m and $\text{MAE}_{\text{AW3D30V3}}=1.9$ m when slope$\leq1^\circ$ whereas $\text{MAE}_{\text{NASADEM}}=2.0$ m and $\text{MAE}_{\text{AW3D30V3}}=2.2$

m when 1°<slope≤5°). The GDEM3 also improved the vertical accuracy of GDEM2, as the aspect-based interquartile range shift caused by slope increase observed on GDEM2 is diminished on GDEM3. However, despite the vertical accuracy improvement of GDEM3, it still has larger MAE values and more dispersion than AW3D30 and NASADEM.

The results obtained show that an adequate vertical accuracy assessment of DSMs needs to consider the spatial distribution of GCPs, Difference of DSMs (DoDs) and derivatives of DSMs (i.e., slope and aspect) as the use of DoDs provide information on DSM errors (i.e. interpolation artefacts) that can not be assessed through the use of geodetic benchmarks and because DSM errors depend on both slope and aspect.

Acknowledgements

Funding for this work was provided by UNAM through project grant PAPIIT-IN110720. ALOS AW3D30 provided by JAXA©. ASTER GDEM is a product of METI and NASA. SRTM data (SRTMGL1-V003) courtesy of the NASA EOSDIS Land Processes Distributed Active Archive Center (LP DAAC), USGS/Earth Resources Observation and Science (EROS) Center, Sioux Falls, South Dakota.

References

Abrams, M., Crippen, R., and Fujisada, H. (2020). ASTER Global Digital Elevation Model (GDEM) and ASTER Global Water Body Dataset (ASTWBD). *Remote Sensing*, 12(7):1–12.

Berry, P. A. M., Garlick, J. D., and Smith, R. G. (2007). Near-global validation of the SRTM DEM using satellite radar altimetry. 106:17–27.

Bivand, R., Krug, R., Neteler, M., and Jeworutzki, S. (2019). rgrass7: Interface Between GRASS 7 Geographical Information System and R. R package version 0.2-1.

Bolkas, D., Fotopoulos, G., Braun, A., and Tziavos, I. N. (2016). Assessing digital elevation model uncertainty using GPS survey data. *Journal of Surveying Engineering*, 142(3):1–8.

Buckley, S. M., Agram, P. S., Belz, J. E., Crippen, R. E., Gurrola, E. M., Hensley, S., Kobrick, M., Lavalle, M., Martin, J. M., Neumann, M., Nguyen, Q. D., Rosen, P. A., Shimada, J. G., Simard, M., and Tung, W. W. (2020). NASADEM: User Guide. Technical Report January.

Callow, J. N., Van Niel, K. P., and Boggs, G. S. (2007). How does modifying a DEM to reflect known hydrology affect subsequent terrain analysis? *Journal of Hydrology*, 332(1-2):30–39.

Capra, L., Manea, V. C., Manea, M., and Norini, G. (2011). The importance of digital elevation model resolution on granular flow simulations: a test case for Colima volcano using TITAN2D computational routine. *Natural Hazards*, 59(2):665–680.

Carabajal, C. C. and Boy, J. P. (2016). Evaluation of ASTER GDEM V3 using ICESat laser altimetry. *International Archives of the Photogrammetry, Remote Sensing and Spatial Information Sciences - ISPRS Archives*, 41(June):117–124.

Carr, D. B., Littlefield, R. J., Nicholson, W. L., and Littlefield, J. S. (1987). Scatterplot matrix techniques for large N. *Journal of the American Statistical Association*, 82(398):424–436.

Carrera-Hernández, J. and Gaskin, S. (2007). Spatio temporal analysis of daily precipitation and temperature in the Basin of Mexico. *Journal of Hydrology*, 336(3-4):231–249.

Carrera-Hernández, J. and Gaskin, S. (2008a). Spatio-temporal analysis of potential aquifer recharge: Application to the Basin of Mexico. *Journal of Hydrology*, 353(3-4):228–246.

Carrera-Hernández, J. and Gaskin, S. (2008b). The Basin of Mexico Hydrogeological Database (BMHDB): Implementation, queries and interaction with open source software. *Environmental Modelling & Software*, 23(10-11):1271–1279.

Carrera-Hernandez, J. J. (2018). A tale of Mexico's most exploited-and connected-watersheds: the Basin of Mexico and the Lerma-Chapala Basin. *Wiley Interdisciplinary Reviews: Water*, 5(1):e1247.

Carrera-Hernández, J. J. (2020a). Vertical datum transformation grids for Mexico. *Scientific Data*, 7(167):1—-10.

Carrera-Hernández, J. J. (2020b). Vertical Datum transformation grids for Mexico dataset.

Carrera-Hernández, J. J., Carreón-Freyre, D., Cerca-Martínez, M., and Levresse, G. (2016). Groundwater flow in a transboundary fault-dominated aquifer and the importance of regional modeling: the case of the city of Querétaro, Mexico. *Hydrogeology Journal*, 24(2):373–393.

Chirico, P., Malpeli, K., and Trimble, S. (2012). Accuracy evaluation of an ASTER-derived global digital elevation model (GDEM) version 1 and version 2 for two sites in Western Africa. *GIScience and Remote Sensing*, 49(6):775–801.

Conway, J., Eddelbuettel, D., Nishiyama, T., Kumar, S., and Tiffin, N. (2017). RPostgreSQL: R Interface to the 'PostgreSQL' Database System. R package version 0.6-2.

Emeis, S. and Knoche, H. R. (2009). Applications in Meteorology. In *Developments in Soil Science, Volume 33: Geomorphometry: Concepts, Software, Applications*, chapter 26, pages 603—-622.

Escobar-Flores, J. G., Lopez-Sanchez, C. A., Sandoval, S., Marquez-Linares, M. A., and Wehenkel, C. (2018). Predicting Pinus monophylla forest cover in the Baja California Desert by remote sensing. *PeerJ*, 2018(4):1–17.

Farr, T. G., Rosen, P. A., Caro, E., Crippen, R., Duren, R., Hensley, S., Kobrick, M., Paller, M., Rodriguez, E., Roth, L., Seal, D., Shaffer, S., Shimada, J., Umland, J., Werner, M., Oskin, M., Burbank, D., and Alsdorf, D. (2007). The Shuttle Radar Topography Mission. *Reviews of Geophysics*, 45(2):1–33.

Fisher, P. F. and Tate, N. J. (2006). Causes and consequences of error in digital elevation models. *Progress in Physical Geography*, 30(4):467–489.

Florinsky, I. V. (2017). An illustrated introduction to general geomorphometry. *Progress in Physical Geography: Earth and Environment*, 41(6):723–752.

Gantenbein, C. (2012). Creating Shaded Relief for Geologic Mapping using Multiple Light Sources. Technical report.

Gesch, D., Oimoen, M., Danielson, J., and Meyer, D. (2016). Validation of the ASTER global digital elevation model version 3 over the Conterminous United States. In *International Archives of the Photogrammetry, Remote Sensing and Spatial Information Sciences - ISPRS Archives*, volume 41, pages 143–148.

Gesch, D. B. (2018). Best practices for elevation-based assessments of sea-level rise and coastal flooding exposure. *Frontiers in Earth Science*, 6(December).

GRASS Development Team (2020). GRASS GIS 7.8.3 software. Technical report, Open Source Geospatial Foundation.

Grayson, R. B. and Blöschl, G. (2001). *Spatial Patterns in Catchment Hydrology: Observations and Modelling*. 1 edition.

Griffin, J., Latief, H., Kongko, W., Harig, S., Horspool, N., Hanung, R., Rojali, A., Maher, N., Fuchs, A., Hossen, J., Upi, S., Edi Dewanto, S., Rakowsky, N., and Cummins, P. (2015). An evaluation of onshore digital elevation models for modeling tsunami inundation zones. *Frontiers in Earth Science*, 3(June):1–16.

Grohmann, C. H. (2018). Evaluation of TanDEM-X DEMs on selected Brazilian sites: Comparison with SRTM, ASTER GDEM and ALOS AW3D30. *Remote Sensing of Environment*, 212(May):121–133.

Hayakawa, Y. S., Oguchi, T., and Lin, Z. (2008). Comparison of new and existing global digital elevation models: ASTER G-DEM and SRTM-3. *Geophysical Research Letters*, 35(17):L17404.

Hengl, T. and Evans, I. S. (2009). Mathematical and digital models of the land surface. In Hengl, T. and Reuter, H. I., editors, *Geomorphometry: Concepts, Software, and Applications*, volume 33, chapter 2, pages 31–63. Elsevier.

Hirt, C. (2018). Artefact detection in global digital elevation models (DEMs): The Maximum Slope Approach and its application for complete screening of the SRTM v4.1 and MERIT DEMs. *Remote Sensing of Environment*, 207(September 2017):27–41.

Hirt, C., Filmer, M. S., and Featherstone, W. E. (2010). Comparison and validation of the recent freely available ASTER-GDEM ver1, SRTM ver4.1 and GEODATA DEM-9s ver3 digital elevation models over Australia. *Australian Journal of Earth Sciences*, 57(3):337–347.

Höhle, J. and Höhle, M. (2009). Accuracy assessment of digital elevation models by means of robust statistical methods. *ISPRS Journal of Photogrammetry and Remote Sensing*, 64(4):398–406.

Hubbard, B. E., Sheridan, M. F., Carrasco-Núñez, G., Díaz-Castellón, R., and Rodríguez, S. R. (2007). Comparative lahar hazard mapping at Volcan Citlaltépetl, Mexico using SRTM, ASTER and DTED-1 digital topographic data. *Journal of Volcanology and Geothermal Research*, 160(1-2):99–124.

Huggel, C., Schneider, D., Miranda, P. J., Delgado Granados, H., and Kääb, A. (2008). Evaluation of ASTER and SRTM DEM data for lahar modeling: A case study on lahars from Popocatépetl Volcano, Mexico. *Journal of Volcanology and Geothermal Research*, 170(1-2):99–110.

Hutchinson, M. (2011). User guide.

Hvidegaard, S. M., Sandberg Sørensen, L., and Forsberg, R. (2012). ASTER GDEM validation using LiDAR data over coastal regions of Greenland. *Remote Sensing Letters*, 3(1):85–91.

INEGI (2015). Guía Metodológica de la Red Geodésica Horizontal. Technical report.

Ioannidis, C., Xinogalas, E., and Soile, S. (2014). Assessment of the global digital elevation models aster and srtm in Greece. *Survey Review*, 46(338):342.

Lacan, P., Ortuño, M., Audin, L., Perea, H., Baize, S., Aguirre-Díaz, G., and Zúñiga, F. R. (2018). Sedimentary evidence of historical and prehistorical earthquakes along the Venta de Bravo Fault System, Acambay Graben (Central Mexico). *Sedimentary Geology*, 365:62–77.

Lehner, B., Verdin, K., and Jarvis, A. (2008). New global hydrography derived from spaceborne elevation data. *Eos*, 89(10):93–94.

Li, P., Li, Z., Muller, J.-P., Shi, C., and Liu, J. (2015). A new quality validation of global digital elevation models freely available in China. *Survey Review*, 48(351):409–420.

Li, P., Shi, C., Li, Z., Muller, J. P., Drummond, J., Li, X., Li, T., Li, Y., and Liu, J. (2013). Evaluation of ASTER GDEM using GPS benchmarks and SRTM in China. *International Journal of Remote Sensing*, 34(5):1744–1771.

Liu, J. K., Chang, K. T., Lin, C., and Chang, L. C. (2015). Accuracy evaluation of ALOS DEM with airborne LiDAR data in Southern Taiwan. *International Geoscience and Remote Sensing Symposium (IGARSS)*, 2015-Novem:3025–3028.

López-Alvis, J., Carrera-Hernández, J. J., Levresse, G., and Nieto-Samaniego, Á. F. (2019). Assessment of groundwater depletion caused by excessive extraction through groundwater flow modeling: the Celaya aquifer in central Mexico. *Environmental Earth Sciences*, 78(15):1–22.

Mendoza-Ponce, A., Figueroa-Soto, A., Soria-Caballero, D., and Garduño-Monroy, V. H. (2018). Active faults sources for the Pátzcuaro-Acambay fault system (Mexico): Fractal analysis of slip rates and magnitudes Mw estimated from fault length. *Natural Hazards and Earth System Sciences*, 18(11):3121–3135.

Moreno-Madriñán, M., Crosson, W., Eisen, L., Estes, S., Estes Jr., M., Hayden, M., Hemmings, S., Irwin, D., Lozano-Fuentes, S., Monaghan, A., Quattrochi, D., Welsh-Rodriguez, C., and Zielinski-Gutierrez, E. (2014). Correlating Remote Sensing Data with the Abundance of Pupae of the Dengue Virus Mosquito Vector, Aedes aegypti, in Central Mexico. *ISPRS International Journal of Geo-Information*, 3(2):732–749.

Mukul, M., Srivastava, V., Jade, S., and Mukul, M. (2017). Uncertainties in the Shuttle Radar Topography Mission (SRTM) Heights: Insights from the Indian Himalaya and Peninsula. *Scientific Reports*, 7(February 2016):1–10.

Muñoz-salinas, E., Castillo-rodríguez, M., Manea, V., Manea, M., and Palacios, D. (2009). Lahar fl ow simulations using LAHARZ program : Application for the Popocatépetl volcano , Mexico. *Journal of Volcanology and Geothermal Research*, 182(1-2):13–22.

NALCMS (2020). 2010 Land Cover of North America at 30 meters.

NASA (2015). The Shuttle Radar Topography Mission (SRTM) Collection User Guide. Technical report.

Neteler, M., Bowman, M. H., Landa, M., and Metz, M. (2012). GRASS GIS: A multi-purpose open source GIS. *Environmental Modelling and Software*, 31:124–130.

Pike, R., Evans, I., and Hengl, T. (2009). Geomorphometry: A Brief Guide. In Hengl, T. and Reuter, H. I., editors, *Geomorphometry: Concepts, Software, and Applications*, volume 33, chapter 1, pages 3–30. Elsevier.

R Core Team (2020). R: A Language and Environment for Statistical Computing.

Rexer, M. and Hirt, C. (2014). Comparison of free high resolution digital elevation data sets (ASTER GDEM2, SRTM v2.1/v4.1) and validation against accurate heights from the Australian National Gravity Database. *Australian Journal of Earth Sciences*, 61(2):213–226.

Rodríguez, E., Morris, C. S., and Belz, J. E. (2006). A Global Assessment of the SRTM Performance. *Photogrammetric Engineering & Remote Sensing*, 72(3):249–260.

Santillan, J. R. and Makinano-Santillan, M. (2017). Elevation-based sea-level rise vulnerability assessment of Mindanao, philippines: Are freely-available 30-m DEMs good enough? In *International Archives of the Photogrammetry, Remote Sensing and Spatial Information Sciences - ISPRS Archives*, volume 42, pages 543–550.

Satge, F., Denezine, M., Pillco, R., Timouk, F., Pinel, S., Molina, J., Garnier, J., Seyler, F., and Bonnet, M. P. (2016). Absolute and relative height-pixel accuracy of SRTM-GL1 over the South American Andean Plateau. *ISPRS Journal of Photogrammetry and Remote Sensing*, 121:157–166.

Schneider, D., Delgado Granados, H., Huggel, C., and Kääb, A. (2008). Assessing lahars from ice-capped volcanoes using ASTER satellite data, the SRTM DTM and two different flow models: Case study on Iztaccíhuatl (Central Mexico). *Natural Hazards and Earth System Science*, 8(3):559–571.

Shortridge, A. and Messina, J. (2011). Spatial structure and landscape associations of SRTM error. *Remote Sensing of Environment*, 115(6):1576–1587.

Slater, J. A., Heady, B., Kroenung, G., Curtis, W., Haase, J., Hoegemann, D., Shockley, C., and Tracy, K. (2011). Global Assessment of the new ASTER Global Digital Elevation Model. *Photogrammetric Engineering & Remote Sensing*, 77(4):335–349.

Tachikawa, T., Manabu Kaku, Iwasaki, A., Gesch, D., Oimoen, M., Zhang, Z., Danielson, J., Krieger, T., Curtis, B., Haase, J., Abrams, M., Crippen, R., and Carabajal, C.

(2011). ASTER Global Digital Elevation Model Version 2. Summary of validation results. Technical report, NASA Land Processes Distributed Active Archive Center and the Joint Japan-US ASTER Science Team.

Tadono, T., Nagai, H., Ishida, H., Oda, F., Naito, S., Minakawa, K., and Iwamoto, H. (2016). Generation of the 30 M-MESH global digital surface model by ALOS PRISM. In *International Archives of the Photogrammetry, Remote Sensing and Spatial Information Sciences - ISPRS Archives*, volume 41, pages 157–162.

Tadono, T., Shimada, M., Murakami, H., Takaku, J., and Kawamoto, S. (2008). Updated results of calibration and validation of alos optical sensors. *International Geoscience and Remote Sensing Symposium (IGARSS)*, 1(1).

Takaku, J., Futamura, N., Iijima, T., Tadono, T., and Shimada, M. (2007). High resolution DSM generation from ALOS PRISM. *International Geoscience and Remote Sensing Symposium (IGARSS)*, pages 1974–1977.

Takaku, J., Tadono, T., and Tsutsui, K. (2014). Generation of High Resolution Global DSM from ALOS PRISM. *ISPRS - International Archives of the Photogrammetry, Remote Sensing and Spatial Information Sciences*, XL-4(4):243–248.

Takaku, J., Tadono, T., Tsutsui, K., and Ichikawa, M. (2016). Validation of 'AW3D' global DSM generated from ALOS PRISM. In *International Geoscience and Remote Sensing Symposium (IGARSS)*, volume III-4, pages 25–31.

Urai, M., Tachikawa, T., and Fujisada, H. (2012). Data acquisition strategies for ASTER global DEM generation. *ISPRS Annals of the Photogrammetry, Remote Sensing and Spatial Information Sciences*, 1(September):199–202.

Uuemaa, E., Ahi, S., Montibeller, B., Muru, M., and Kmoch, A. (2020). Vertical Accuracy of Freely Available Global Digital Elevation Models (ASTER, AW3D30, MERIT, TanDEM-X, SRTM, and NASADEM). *Remote Sensing*, 12(21):3482.

Varga, M. and Bašić, T. (2015). Accuracy validation and comparison of global digital elevation models over Croatia. *International Journal of Remote Sensing*, 36(1):170–189.

Wechsler, S. P. (2003). Perceptions of Digital Elevation Model Uncertainty by DEM Users. *Journal of the Urban and Regional Information Systems Association*, 15(2):57–64.

Westerhoff, R., White, P., and Miguez-Macho, G. (2018). Application of an improved global-scale groundwater model for water table estimation across New Zealand. *Hydrology and Earth System Sciences*, 22(12):6449–6472.

Wickham, H. (2016). *ggplot2: Elegant Graphics for Data Analysis*. Springer-Verlag, New York, NY.

Willmott, C. J. and Matsuura, K. (2005). Advantages of the mean absolute error (MAE) over the root mean square error (RMSE) in assessing average model performance. *Climate Research*, 30(1):79–82.

Wise, S. (2000). Assessing the quality for hydrological applications of digital elevation models derived from contours. *Hydrological Processes*, 14(11-12):1909–1929.

Zambrano-Bigiarini, M. (2017). hydroGOF: Goodness-of-fit functions for comparison of simulated and observed hydrological time series. R package version 0.3-10.

Supplementary Material

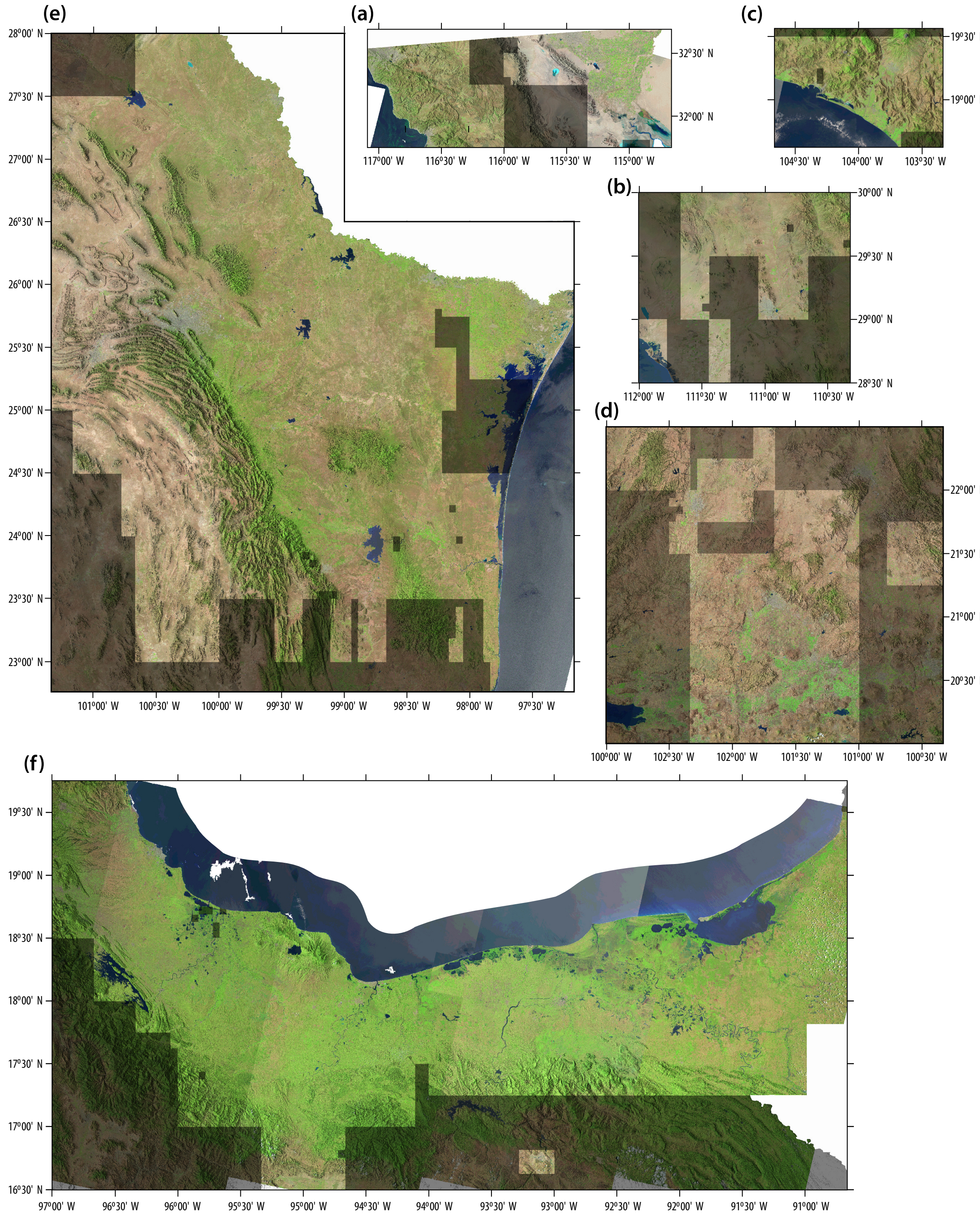

Figure S1: Areas used for the analyses undertaken with LiDAR data: a) Ensenada, b) Sonora, c) Colima, d) Guanajuato, e) Monterrey, and f) Tabasco. These areas were selected in order to have a large number of tiles adjacent to each other, and their location within Mexico is shown in Fig. 3. True color composites of LANDSAT8 imagery overlaid on shaded relief of AW3D30V3, with darkened areas representing areas without LiDAR coverage.

Table S1: Detailed robust statistics of AW3D30 V2 according to variation in both slope and aspect.

		Slope (degrees)													
	Aspect	0–1	1–5	5–10	10–15	15–20	20–25	25–30	30–35	35–40	40–45	45–50	50–55	55–60	>60
Ncells (10^6)	All	115.242	118.250	36.234	20.155	15.488	12.729	10.172	7.523	4.375	1.792	0.700	0.313	0.152	0.118
MAE (m)	E	1.93	2.18	2.43	2.56	2.72	2.87	3.07	3.33	3.78	4.51	5.84	8.11	11.37	21.03
	ENE	1.93	2.18	2.44	2.63	2.82	3.00	3.24	3.54	3.99	4.74	6.28	8.44	11.56	22.09
	NE	1.94	2.20	2.49	2.75	2.99	3.24	3.56	3.96	4.52	5.58	7.35	10.11	14.08	26.07
	NNE	1.93	2.23	2.56	2.88	3.21	3.60	4.04	4.61	5.47	6.91	9.40	13.07	18.00	31.34
	N	1.94	2.28	2.62	3.00	3.42	3.90	4.50	5.26	6.42	8.24	11.21	15.56	21.07	34.94
	NNW	1.98	2.30	2.66	3.10	3.58	4.14	4.85	5.69	6.98	9.09	12.34	17.24	23.77	39.40
	NW	2.01	2.31	2.70	3.18	3.67	4.23	4.93	5.73	6.96	9.01	12.34	17.02	23.63	40.61
	WNW	2.01	2.30	2.73	3.18	3.63	4.13	4.69	5.34	6.29	7.95	10.40	13.95	19.79	35.22
	W	2.00	2.29	2.71	3.08	3.44	3.79	4.19	4.63	5.34	6.54	8.27	10.94	15.03	28.23
	WSW	1.97	2.25	2.61	2.92	3.20	3.46	3.72	4.01	4.51	5.46	6.91	8.96	12.17	21.25
	SW	1.96	2.21	2.52	2.78	3.02	3.23	3.42	3.59	4.02	4.88	6.30	8.41	11.58	20.59
	SSW	1.94	2.20	2.45	2.67	2.90	3.09	3.27	3.47	3.90	4.86	6.40	8.74	12.13	22.94
	S	1.94	2.20	2.41	2.60	2.82	3.00	3.17	3.44	3.99	4.99	6.77	9.31	13.49	26.13
	SSE	1.96	2.20	2.38	2.54	2.74	2.93	3.13	3.40	3.98	5.01	6.81	9.64	13.92	25.89
	SE	1.96	2.20	2.37	2.52	2.71	2.87	3.05	3.34	3.89	4.85	6.57	9.21	13.68	25.72
	ESE	1.94	2.20	2.39	2.53	2.69	2.84	3.04	3.28	3.77	4.62	6.05	8.50	12.35	23.15
	All	1.96	2.23	2.53	2.81	3.10	3.40	3.74	4.16	4.84	6.01	7.95	10.92	15.25	27.24
	min	1.93	2.18	2.37	2.52	2.69	2.84	3.04	3.28	3.77	4.51	5.84	8.11	11.37	20.59
	max	2.01	2.31	2.73	3.18	3.67	4.23	4.93	5.73	6.98	9.09	12.34	17.24	23.77	40.61
	diff	0.08	0.13	0.36	0.66	0.98	1.39	1.89	2.45	3.20	4.58	6.50	9.13	12.41	20.01
Median (m)	E	1.31	1.52	1.44	1.33	1.17	0.95	0.75	0.42	0.04	-0.29	-0.61	-1.12	-1.49	-2.71
	ENE	1.32	1.51	1.49	1.47	1.41	1.31	1.27	1.20	1.07	1.05	1.02	1.25	1.73	3.35
	NE	1.29	1.50	1.56	1.66	1.71	1.80	1.95	2.15	2.38	2.80	3.53	4.73	6.46	11.89
	NNE	1.22	1.50	1.64	1.86	2.08	2.37	2.75	3.23	3.81	4.79	6.21	8.37	11.43	18.42
	N	1.13	1.52	1.75	2.08	2.44	2.88	3.48	4.19	5.15	6.51	8.24	10.68	14.47	22.39
	NNW	1.12	1.55	1.84	2.26	2.70	3.26	3.99	4.81	5.89	7.53	9.52	12.64	17.15	28.02
	NW	1.09	1.58	1.93	2.38	2.86	3.44	4.16	4.95	6.01	7.69	9.77	12.68	17.66	30.48
	WNW	1.07	1.59	1.99	2.41	2.84	3.35	3.95	4.59	5.44	6.89	8.54	10.87	14.29	24.93
	W	1.06	1.60	1.98	2.30	2.59	2.94	3.34	3.74	4.36	5.40	6.60	8.05	10.29	16.08
	WSW	1.08	1.60	1.88	2.07	2.22	2.41	2.59	2.75	3.11	3.74	4.47	5.35	6.60	8.14
	SW	1.11	1.59	1.75	1.82	1.84	1.86	1.84	1.71	1.77	2.14	2.42	2.56	3.05	3.91
	SSW	1.15	1.53	1.63	1.60	1.51	1.38	1.17	0.82	0.60	0.68	0.68	0.68	0.84	1.49
	S	1.17	1.50	1.52	1.43	1.24	0.99	0.61	0.11	-0.27	-0.48	-0.69	-0.94	-1.21	-0.09
	SSE	1.23	1.49	1.45	1.29	1.05	0.75	0.33	-0.24	-0.78	-1.11	-1.59	-2.23	-2.58	-2.64
	SE	1.25	1.51	1.40	1.22	0.97	0.65	0.23	-0.34	-0.93	-1.44	-1.99	-2.85	-3.57	-5.01
	ESE	1.28	1.53	1.40	1.24	1.01	0.73	0.36	-0.11	-0.67	-1.17	-1.71	-2.54	-3.52	-5.21
	All	1.19	1.54	1.66	1.77	1.85	1.95	2.05	2.11	2.26	2.60	2.99	3.64	4.77	7.86
	min	1.06	1.49	1.40	1.22	0.97	0.65	0.23	-0.34	-0.93	-1.44	-1.99	-2.85	-3.57	-5.21
	max	1.32	1.60	1.99	2.41	2.86	3.44	4.16	4.95	6.01	7.69	9.77	12.68	17.66	30.48
	diff	0.26	0.11	0.59	1.19	1.89	2.79	3.93	5.29	6.93	9.13	11.76	15.54	21.22	35.69
NMAD (m)	E	1.80	2.02	2.35	2.56	2.82	3.09	3.39	3.76	4.22	4.92	5.95	7.52	10.31	17.48
	ENE	1.80	2.03	2.33	2.59	2.88	3.17	3.49	3.88	4.37	5.12	6.34	8.13	10.86	18.46
	NE	1.82	2.06	2.33	2.63	2.95	3.25	3.60	4.01	4.53	5.46	6.81	8.93	11.92	21.26
	NNE	1.86	2.06	2.35	2.65	2.99	3.35	3.72	4.16	4.78	5.81	7.56	10.27	14.02	24.62
	N	1.91	2.09	2.35	2.65	3.00	3.37	3.74	4.21	4.89	6.01	8.02	11.31	15.79	26.59
	NNW	1.96	2.09	2.34	2.65	3.01	3.37	3.74	4.18	4.88	6.09	8.25	11.96	16.86	27.80
	NW	2.02	2.08	2.33	2.65	2.99	3.31	3.65	4.05	4.68	5.76	7.70	10.96	15.55	27.91
	WNW	2.03	2.07	2.32	2.61	2.90	3.18	3.45	3.80	4.35	5.15	6.54	8.89	12.90	22.91
	W	2.02	2.06	2.29	2.54	2.79	3.02	3.24	3.55	4.03	4.72	5.79	7.60	10.35	19.03
	WSW	1.98	2.01	2.24	2.47	2.74	2.97	3.22	3.53	3.96	4.70	5.81	7.39	10.03	17.32
	SW	1.95	1.96	2.21	2.47	2.75	3.01	3.30	3.57	4.08	4.89	6.09	7.86	10.54	18.08
	SSW	1.93	1.99	2.23	2.49	2.80	3.07	3.35	3.67	4.18	5.17	6.52	8.59	11.66	20.01
	S	1.93	2.03	2.27	2.51	2.82	3.11	3.37	3.67	4.23	5.22	6.72	9.00	12.60	22.41
	SSE	1.91	2.04	2.30	2.54	2.82	3.10	3.36	3.63	4.17	5.11	6.52	8.79	12.75	23.09
	SE	1.89	2.05	2.32	2.54	2.83	3.08	3.29	3.58	4.07	4.88	6.21	8.21	11.46	21.96
	ESE	1.85	2.04	2.34	2.56	2.82	3.07	3.32	3.62	4.10	4.81	5.91	7.71	10.82	19.61
	All	1.90	2.04	2.31	2.60	2.96	3.35	3.80	4.36	5.14	6.31	7.96	10.47	14.28	24.50
	min	1.80	1.96	2.21	2.47	2.74	2.97	3.22	3.53	3.96	4.70	5.79	7.39	10.03	17.32
	max	2.03	2.09	2.35	2.65	3.01	3.37	3.74	4.21	4.89	6.09	8.25	11.96	16.86	27.91
	diff	0.24	0.13	0.14	0.18	0.27	0.40	0.52	0.68	0.93	1.39	2.46	4.56	6.84	10.59

Table S2: Detailed robust statistics of AW3D30 V3 according to variation in both slope and aspect.

		Slope (degrees)													
	Aspect	0–1	1–5	5–10	10–15	15–20	20–25	25–30	30–35	35–40	40–45	45–50	50–55	55–60	>60
Ncells (10^6)	All	114.957	117.996	36.172	20.127	15.466	12.710	10.152	7.501	4.353	1.773	0.685	0.300	0.140	0.092
MAE (m)	E	1.92	2.18	2.42	2.56	2.71	2.86	3.05	3.30	3.70	4.43	5.66	7.79	10.66	19.22
	ENE	1.92	2.17	2.44	2.63	2.81	2.99	3.22	3.51	3.93	4.67	6.11	8.08	10.95	20.44
	NE	1.92	2.20	2.49	2.74	2.99	3.23	3.55	3.94	4.47	5.49	7.12	9.73	13.27	24.39
	NNE	1.92	2.23	2.55	2.87	3.21	3.59	4.03	4.59	5.42	6.82	9.18	12.68	17.32	29.74
	N	1.93	2.27	2.61	3.00	3.41	3.90	4.49	5.24	6.37	8.14	10.99	15.17	20.48	33.27
	NNW	1.97	2.29	2.66	3.10	3.57	4.13	4.83	5.67	6.93	8.98	12.10	16.64	22.83	37.06
	NW	2.00	2.30	2.70	3.18	3.67	4.22	4.91	5.71	6.92	8.90	11.97	16.45	22.58	37.63
	WNW	2.00	2.29	2.73	3.18	3.62	4.12	4.68	5.33	6.25	7.88	10.18	13.55	18.80	32.59
	W	1.98	2.28	2.70	3.08	3.43	3.79	4.19	4.61	5.31	6.49	8.16	10.68	14.57	26.46
	WSW	1.95	2.24	2.61	2.92	3.19	3.45	3.71	3.99	4.48	5.41	6.81	8.73	11.67	19.41
	SW	1.94	2.21	2.51	2.78	3.01	3.22	3.41	3.57	3.99	4.83	6.15	8.09	10.98	19.24
	SSW	1.93	2.19	2.45	2.67	2.89	3.08	3.25	3.45	3.86	4.79	6.24	8.42	11.58	21.74
	S	1.93	2.20	2.41	2.60	2.81	3.00	3.16	3.41	3.93	4.89	6.56	8.96	12.96	24.87
	SSE	1.94	2.20	2.38	2.54	2.73	2.92	3.11	3.37	3.93	4.89	6.57	9.13	13.15	24.70
	SE	1.94	2.20	2.37	2.52	2.70	2.86	3.03	3.31	3.84	4.75	6.33	8.70	12.69	24.16
	ESE	1.92	2.20	2.39	2.52	2.68	2.84	3.02	3.25	3.72	4.52	5.87	8.06	11.56	21.28
	All	1.94	2.23	2.52	2.80	3.09	3.39	3.73	4.13	4.79	5.92	7.74	10.51	14.51	25.55
	min	1.92	2.17	2.37	2.52	2.68	2.84	3.02	3.25	3.70	4.43	5.66	7.79	10.66	19.22
	max	2.00	2.30	2.73	3.18	3.67	4.22	4.91	5.71	6.93	8.98	12.10	16.64	22.83	37.63
	diff	0.08	0.13	0.36	0.66	0.98	1.39	1.89	2.46	3.23	4.55	6.44	8.85	12.17	18.41
Median (m)	E	1.32	1.52	1.44	1.33	1.17	0.95	0.75	0.42	0.03	-0.30	-0.60	-1.11	-1.44	-2.49
	ENE	1.33	1.51	1.49	1.47	1.41	1.31	1.27	1.20	1.07	1.05	1.01	1.25	1.72	2.88
	NE	1.29	1.50	1.56	1.66	1.71	1.80	1.95	2.15	2.38	2.80	3.51	4.65	6.35	10.72
	NNE	1.22	1.50	1.64	1.86	2.08	2.37	2.75	3.23	3.81	4.78	6.20	8.30	11.13	17.38
	N	1.13	1.52	1.75	2.08	2.44	2.88	3.48	4.19	5.14	6.50	8.19	10.65	14.37	21.15
	NNW	1.12	1.55	1.84	2.26	2.70	3.26	3.99	4.81	5.88	7.51	9.47	12.46	16.67	26.01
	NW	1.09	1.58	1.93	2.38	2.86	3.44	4.15	4.95	6.00	7.66	9.71	12.48	17.26	28.41
	WNW	1.07	1.59	1.99	2.41	2.84	3.35	3.95	4.59	5.43	6.87	8.53	10.75	13.82	22.95
	W	1.06	1.61	1.98	2.30	2.59	2.94	3.34	3.74	4.36	5.40	6.59	8.01	10.13	15.01
	WSW	1.08	1.60	1.88	2.07	2.22	2.41	2.59	2.75	3.11	3.75	4.48	5.30	6.55	7.71
	SW	1.11	1.59	1.75	1.82	1.84	1.86	1.84	1.71	1.78	2.14	2.41	2.55	2.90	3.73
	SSW	1.15	1.53	1.63	1.60	1.51	1.38	1.17	0.82	0.60	0.68	0.68	0.68	0.87	1.65
	S	1.17	1.50	1.52	1.43	1.24	0.99	0.61	0.11	-0.28	-0.49	-0.68	-0.94	-1.12	0.07
	SSE	1.24	1.49	1.45	1.29	1.05	0.75	0.33	-0.24	-0.79	-1.11	-1.58	-2.21	-2.45	-1.97
	SE	1.26	1.51	1.40	1.22	0.97	0.65	0.23	-0.34	-0.93	-1.44	-1.97	-2.81	-3.44	-4.73
	ESE	1.28	1.53	1.40	1.24	1.01	0.73	0.36	-0.12	-0.68	-1.17	-1.70	-2.54	-3.43	-5.18
	All	1.20	1.54	1.66	1.77	1.85	1.95	2.05	2.11	2.25	2.59	2.96	3.57	4.67	7.41
	min	1.06	1.49	1.40	1.22	0.97	0.65	0.23	-0.34	-0.93	-1.44	-1.97	-2.81	-3.44	-5.18
	max	1.33	1.61	1.99	2.41	2.86	3.44	4.15	4.95	6.00	7.66	9.71	12.48	17.26	28.41
	diff	0.26	0.11	0.59	1.19	1.89	2.79	3.93	5.29	6.93	9.10	11.68	15.28	20.70	33.59
NMAD (m)	E	1.80	2.02	2.34	2.56	2.82	3.09	3.38	3.76	4.21	4.90	5.88	7.41	9.92	15.99
	ENE	1.80	2.03	2.33	2.59	2.88	3.16	3.49	3.88	4.36	5.10	6.29	8.02	10.60	16.98
	NE	1.82	2.06	2.33	2.63	2.94	3.25	3.59	4.01	4.52	5.43	6.75	8.81	11.52	19.33
	NNE	1.86	2.06	2.35	2.65	2.99	3.35	3.71	4.15	4.77	5.79	7.49	10.04	13.49	22.96
	N	1.90	2.09	2.35	2.65	3.00	3.37	3.73	4.20	4.88	5.98	7.92	11.04	15.34	25.11
	NNW	1.96	2.09	2.34	2.65	3.01	3.37	3.74	4.17	4.87	6.06	8.16	11.70	16.40	25.94
	NW	2.02	2.08	2.33	2.65	2.98	3.31	3.65	4.04	4.67	5.74	7.61	10.68	14.94	25.70
	WNW	2.03	2.07	2.32	2.61	2.90	3.17	3.44	3.80	4.34	5.13	6.47	8.71	12.12	21.01
	W	2.02	2.06	2.29	2.53	2.78	3.01	3.24	3.54	4.02	4.70	5.75	7.51	10.13	17.31
	WSW	1.98	2.00	2.23	2.47	2.74	2.97	3.21	3.52	3.95	4.68	5.76	7.27	9.56	15.79
	SW	1.95	1.96	2.21	2.47	2.75	3.01	3.29	3.56	4.07	4.87	6.02	7.72	10.21	16.67
	SSW	1.93	1.99	2.23	2.49	2.79	3.07	3.35	3.66	4.17	5.14	6.47	8.42	11.27	18.43
	S	1.93	2.03	2.27	2.51	2.82	3.11	3.36	3.66	4.21	5.19	6.66	8.83	12.17	20.88
	SSE	1.91	2.04	2.30	2.53	2.82	3.10	3.35	3.62	4.15	5.07	6.44	8.58	12.17	21.83
	SE	1.89	2.05	2.32	2.54	2.83	3.07	3.29	3.57	4.06	4.85	6.13	8.00	11.04	20.07
	ESE	1.84	2.04	2.34	2.56	2.82	3.07	3.31	3.61	4.09	4.79	5.85	7.52	10.27	17.46
	All	1.90	2.04	2.31	2.60	2.95	3.34	3.79	4.35	5.13	6.28	7.89	10.27	13.78	22.65
	min	1.80	1.96	2.21	2.47	2.74	2.97	3.21	3.52	3.95	4.68	5.75	7.27	9.56	15.79
	max	2.03	2.09	2.35	2.65	3.01	3.37	3.74	4.20	4.88	6.06	8.16	11.70	16.40	25.94
	diff	0.24	0.13	0.14	0.18	0.27	0.40	0.52	0.68	0.93	1.38	2.42	4.42	6.85	10.15

Table S3: Detailed robust statistics of NASADEM according to variation in both slope and aspect.

		Slope (degrees)													
	Aspect	0-1	1-5	5-10	10–15	15-20	20–25	25–30	30–35	35-40	40-45	45-50	50-55	55-60	>60
Ncells (10^6)	All	117.494	122.108	38.657	21.447	16.398	13.422	10.642	7.763	4.442	1.784	0.672	0.286	0.130	0.088
MAE (m)	E	1.55	2.00	3.28	4.65	5.79	6.93	8.31	10.09	12.49	15.65	20.52	27.12	36.37	53.52
	ENE	1.56	1.96	3.10	4.24	5.11	5.90	6.81	8.03	9.77	12.50	17.25	23.80	31.83	49.15
	NE	1.57	1.96	3.03	4.08	4.84	5.47	6.06	6.80	8.02	10.32	14.08	19.83	26.12	42.23
	NNE	1.59	2.00	3.12	4.28	5.22	6.00	6.71	7.42	8.44	10.33	13.62	18.22	24.32	39.86
	N	1.60	2.07	3.30	4.72	5.96	7.09	8.16	9.24	10.49	12.30	15.37	19.58	24.93	40.18
	NNW	1.64	2.12	3.49	5.14	6.64	8.06	9.46	10.94	12.57	14.84	18.18	22.21	28.80	44.10
	NW	1.67	2.13	3.56	5.31	6.91	8.43	9.99	11.73	13.82	16.24	19.84	24.59	29.53	46.21
	WNW	1.68	2.10	3.45	5.14	6.67	8.14	9.64	11.36	13.44	16.02	19.48	24.24	30.75	44.45
	W	1.69	2.05	3.23	4.73	6.05	7.28	8.58	9.99	11.64	14.08	17.62	22.61	29.61	43.07
	WSW	1.69	2.00	3.02	4.26	5.27	6.19	7.15	8.17	9.46	11.37	14.46	19.22	25.90	40.35
	SW	1.68	1.99	2.93	3.98	4.78	5.43	6.07	6.80	7.86	9.66	12.42	16.34	22.49	37.42
	SSW	1.64	2.01	3.01	4.10	4.89	5.56	6.15	6.80	7.84	9.73	12.49	16.62	21.53	37.28
	S	1.61	2.03	3.21	4.50	5.53	6.41	7.20	8.14	9.48	11.36	14.10	18.50	23.66	39.89
	SSE	1.60	2.06	3.42	4.92	6.18	7.36	8.59	10.01	11.82	14.23	17.62	22.50	28.84	46.04
	SE	1.59	2.07	3.51	5.12	6.51	7.88	9.43	11.33	13.77	16.73	21.03	26.48	32.92	50.60
	ESE	1.57	2.06	3.45	5.00	6.37	7.73	9.38	11.46	14.06	17.38	22.12	28.33	35.50	51.85
	All	1.61	2.03	3.25	4.63	5.77	6.83	7.91	9.15	10.75	13.05	16.57	21.49	27.81	43.55
	min	1.55	1.96	2.93	3.98	4.78	5.43	6.06	6.80	7.84	9.66	12.42	16.34	21.53	37.28
	max	1.69	2.13	3.56	5.31	6.91	8.43	9.99	11.73	14.06	17.38	22.12	28.33	36.37	53.52
	diff	0.14	0.18	0.63	1.33	2.12	3.00	3.93	4.94	6.22	7.72	9.70	11.99	14.84	16.24
Median (m)	E	-0.18	0.28	1.25	2.40	3.56	4.85	6.37	8.15	10.14	12.25	15.43	19.97	27.10	39.55
	ENE	-0.22	0.08	0.63	1.26	1.90	2.64	3.51	4.63	5.86	6.93	8.92	11.87	16.84	29.36
	NE	-0.27	-0.17	-0.16	-0.19	-0.20	-0.14	0.04	0.42	0.94	1.24	1.66	3.33	5.48	12.61
	NNE	-0.33	-0.43	-0.94	-1.63	-2.30	-2.89	-3.41	-3.77	-3.94	-4.15	-4.22	-3.42	-1.52	3.32
	N	-0.36	-0.66	-1.59	-2.83	-4.05	-5.22	-6.31	-7.27	-7.98	-8.65	-9.05	-8.79	-6.53	-0.62
	NNW	-0.39	-0.81	-2.06	-3.66	-5.26	-6.80	-8.25	-9.60	-10.70	-11.67	-12.51	-12.27	-9.92	-3.15
	NW	-0.41	-0.85	-2.23	-3.99	-5.75	-7.41	-9.00	-10.44	-11.63	-12.26	-12.23	-10.94	-6.42	4.21
	WNW	-0.39	-0.79	-2.08	-3.79	-5.48	-7.09	-8.58	-9.84	-10.69	-10.69	-9.41	-6.03	-0.02	12.77
	W	-0.36	-0.63	-1.69	-3.16	-4.62	-5.99	-7.27	-8.32	-8.81	-8.35	-6.84	-2.83	2.31	14.40
	WSW	-0.33	-0.40	-1.11	-2.15	-3.22	-4.22	-5.15	-5.89	-6.22	-5.92	-5.05	-3.23	0.59	6.74
	SW	-0.28	-0.15	-0.38	-0.87	-1.41	-1.90	-2.34	-2.70	-2.77	-2.79	-2.70	-2.40	-2.19	-3.28
	SSW	-0.23	0.06	0.40	0.56	0.59	0.65	0.73	0.92	1.12	0.92	0.74	0.22	-0.81	-1.85
	S	-0.19	0.23	1.10	1.89	2.55	3.20	3.85	4.65	5.26	5.43	5.51	6.10	5.99	6.43
	SSE	-0.17	0.35	1.59	2.84	3.98	5.12	6.39	7.83	9.31	10.69	12.27	14.64	17.60	25.82
	SE	-0.15	0.42	1.78	3.25	4.63	6.11	7.86	9.89	12.18	14.47	17.55	21.54	25.55	35.47
	ESE	-0.16	0.41	1.66	3.09	4.51	6.04	7.87	10.08	12.50	15.11	18.76	23.00	28.90	38.84
	All	-0.27	-0.17	-0.28	-0.56	-0.88	-1.15	-1.29	-1.14	-0.62	0.05	1.07	2.68	5.57	12.31
	min	-0.41	-0.85	-2.23	-3.99	-5.75	-7.41	-9.00	-10.44	-11.63	-12.26	-12.51	-12.27	-9.92	-3.28
	max	-0.15	0.42	1.78	3.25	4.63	6.11	7.87	10.08	12.50	15.11	18.76	23.00	28.90	39.55
	diff	0.25	1.27	4.00	7.25	10.38	13.52	16.87	20.52	24.13	27.37	31.27	35.27	38.82	42.83
NMAD (m)	E	1.76	2.23	3.48	4.71	5.62	6.28	6.94	7.74	9.07	11.41	15.19	20.92	28.68	42.60
	ENE	1.77	2.19	3.40	4.61	5.52	6.24	6.97	7.82	9.16	11.66	15.97	22.52	29.60	45.51
	NE	1.78	2.18	3.34	4.56	5.51	6.30	6.98	7.82	9.00	11.14	14.76	20.56	27.45	42.67
	NNE	1.78	2.19	3.30	4.51	5.46	6.24	6.92	7.61	8.65	10.54	13.78	18.71	25.77	40.57
	N	1.79	2.21	3.28	4.45	5.40	6.15	6.82	7.56	8.70	10.46	13.72	18.52	26.06	42.80
	NNW	1.82	2.23	3.26	4.42	5.35	6.10	6.86	7.80	9.11	11.17	14.92	20.35	29.37	46.99
	NW	1.85	2.24	3.24	4.39	5.26	5.98	6.84	8.07	9.85	12.64	17.46	24.21	32.99	52.51
	WNW	1.87	2.22	3.20	4.31	5.11	5.79	6.57	7.89	9.98	13.41	18.76	26.15	35.33	49.25
	W	1.87	2.21	3.15	4.24	5.00	5.56	6.22	7.32	9.25	12.44	17.38	24.63	34.57	47.82
	WSW	1.88	2.22	3.13	4.23	5.01	5.61	6.25	7.12	8.60	10.98	14.60	20.49	28.52	44.73
	SW	1.87	2.24	3.20	4.36	5.25	5.91	6.52	7.29	8.47	10.33	13.05	17.41	23.82	38.93
	SSW	1.84	2.26	3.32	4.58	5.54	6.31	6.97	7.69	8.84	10.77	13.46	17.61	22.84	36.88
	S	1.82	2.29	3.45	4.77	5.85	6.63	7.23	7.96	9.40	11.68	14.70	19.45	25.19	39.09
	SSE	1.81	2.31	3.56	4.90	5.96	6.76	7.42	8.15	9.56	11.86	15.37	20.44	26.53	40.76
	SE	1.80	2.32	3.60	4.94	5.94	6.69	7.26	7.95	9.15	11.19	14.34	18.81	25.39	39.53
	ESE	1.78	2.30	3.56	4.84	5.81	6.50	7.11	7.76	8.83	10.89	14.28	18.79	24.62	37.73
	All	1.81	2.29	3.71	5.47	7.01	8.44	9.90	11.47	13.26	15.54	19.07	24.17	31.04	46.16
	min	1.76	2.18	3.13	4.23	5.00	5.56	6.22	7.12	8.47	10.33	13.05	17.41	22.84	36.88
	max	1.88	2.32	3.60	4.94	5.96	6.76	7.42	8.15	9.98	13.41	18.76	26.15	35.33	52.51
	diff	0.11	0.15	0.47	0.71	0.95	1.20	1.20	1.03	1.51	3.07	5.71	8.74	12.49	15.63

Table S4: Detailed robust statistics of SRTM according to variation in both slope and aspect.

		Slope (degrees)													
	Aspect	0-1	1-5	5-10	10-15	15-20	20-25	25-30	30-35	35-40	40-45	45-50	50-55	55-60	>60
Ncells (10^6)	All	117.447	122.023	38.562	21.377	16.340	13.358	10.559	7.641	4.292	1.666	0.594	0.233	0.096	0.052
MAE (m)	E	2.18	2.65	3.77	4.89	5.93	7.01	8.24	9.70	11.49	13.95	17.93	23.93	32.98	51.17
	ENE	2.21	2.75	4.07	5.30	6.39	7.50	8.76	10.32	12.20	14.80	19.17	25.47	34.16	50.86
	NE	2.25	2.87	4.35	5.73	6.91	8.11	9.51	11.30	13.44	16.23	20.49	26.55	34.79	49.76
	NNE	2.29	2.98	4.56	6.08	7.40	8.78	10.38	12.35	14.77	17.75	21.93	27.97	36.03	52.15
	N	2.33	3.05	4.64	6.24	7.63	9.08	10.76	12.80	15.34	18.46	22.79	28.64	36.44	53.56
	NNW	2.37	3.05	4.58	6.13	7.50	8.86	10.46	12.31	14.83	18.13	22.60	28.32	35.83	51.67
	NW	2.39	2.97	4.40	5.86	7.13	8.37	9.80	11.57	14.05	17.68	22.64	28.30	35.60	50.34
	WNW	2.38	2.84	4.16	5.56	6.78	7.98	9.29	11.07	13.46	17.25	22.53	29.28	37.18	52.38
	W	2.35	2.72	3.91	5.24	6.45	7.68	9.05	10.73	12.94	16.22	20.85	27.09	35.08	51.93
	WSW	2.31	2.60	3.68	4.94	6.13	7.38	8.77	10.39	12.30	14.82	18.21	23.00	29.90	43.16
	SW	2.29	2.53	3.48	4.66	5.88	7.12	8.55	10.23	12.00	14.08	17.03	21.23	26.88	41.42
	SSW	2.24	2.51	3.31	4.45	5.65	6.97	8.54	10.35	12.18	14.26	17.27	21.23	26.47	39.43
	S	2.22	2.52	3.22	4.28	5.45	6.75	8.33	10.12	11.92	14.07	16.90	20.51	25.17	36.55
	SSE	2.21	2.53	3.22	4.22	5.31	6.46	7.84	9.40	11.08	13.13	15.86	19.60	24.39	36.32
	SE	2.19	2.56	3.33	4.32	5.33	6.34	7.49	8.83	10.40	12.48	15.58	19.41	24.61	37.78
	ESE	2.18	2.59	3.52	4.54	5.55	6.56	7.71	9.07	10.70	12.96	16.31	21.11	28.05	41.57
	All	2.27	2.72	3.88	5.16	6.35	7.58	9.01	10.72	12.78	15.48	19.34	24.66	31.87	47.24
	min	2.18	2.51	3.22	4.22	5.31	6.34	7.49	8.83	10.40	12.48	15.58	19.41	24.39	36.32
	max	2.39	3.05	4.64	6.24	7.63	9.08	10.76	12.80	15.34	18.46	22.79	29.28	37.18	53.56
	diff	0.21	0.54	1.42	2.02	2.32	2.75	3.27	3.97	4.94	5.98	7.21	9.87	12.79	17.24
Median (m)	E	1.15	1.53	1.86	1.96	2.04	2.26	2.56	2.95	3.44	3.93	5.43	8.57	17.36	33.71
	ENE	1.19	1.69	2.51	3.14	3.73	4.47	5.37	6.50	7.74	8.99	11.41	16.36	25.10	41.12
	NE	1.22	1.84	3.06	4.13	5.15	6.31	7.76	9.56	11.41	13.30	16.25	20.95	27.94	38.95
	NNE	1.19	1.96	3.41	4.79	6.06	7.54	9.31	11.43	13.74	16.21	19.16	23.74	30.29	43.15
	N	1.13	2.01	3.50	4.97	6.32	7.85	9.71	11.86	14.32	16.97	20.29	24.65	30.92	44.39
	NNW	1.13	1.96	3.30	4.60	5.81	7.20	8.92	10.82	13.15	15.92	19.21	23.50	29.96	41.41
	NW	1.09	1.81	2.84	3.77	4.63	5.65	6.95	8.49	10.60	13.67	17.41	22.28	28.53	39.79
	WNW	1.00	1.59	2.23	2.67	2.98	3.38	3.94	4.83	6.50	10.09	15.05	21.00	28.73	42.80
	W	0.92	1.37	1.58	1.38	1.05	0.72	0.48	0.47	1.17	3.84	7.84	14.16	21.20	39.46
	WSW	0.85	1.15	0.92	0.14	-0.79	-1.74	-2.68	-3.56	-3.94	-3.06	-1.51	-0.69	3.02	12.60
	SW	0.83	1.00	0.42	-0.80	-2.16	-3.59	-5.09	-6.73	-7.93	-8.28	-8.88	-9.99	-11.85	-16.50
	SSW	0.83	0.92	0.15	-1.30	-2.92	-4.63	-6.56	-8.56	-10.15	-11.18	-12.55	-14.64	-17.59	-22.75
	S	0.87	0.97	0.11	-1.34	-2.97	-4.71	-6.71	-8.72	-10.24	-11.55	-12.75	-13.96	-15.10	-12.93
	SSE	0.97	1.06	0.28	-1.00	-2.41	-3.89	-5.56	-7.26	-8.59	-9.62	-10.46	-11.04	-11.02	-8.47
	SE	1.04	1.20	0.66	-0.27	-1.30	-2.31	-3.39	-4.50	-5.34	-6.11	-7.04	-7.40	-7.37	-4.97
	ESE	1.09	1.37	1.22	0.76	0.27	-0.13	-0.48	-0.81	-1.10	-1.38	-1.45	-0.64	0.26	9.20
	All	1.04	1.46	1.73	1.76	1.71	1.75	1.89	2.21	3.06	4.37	6.23	9.52	14.90	26.15
	min	0.83	0.92	0.11	-1.34	-2.97	-4.71	-6.71	-8.72	-10.24	-11.55	-12.75	-14.64	-17.59	-22.75
	max	1.22	2.01	3.50	4.97	6.32	7.85	9.71	11.86	14.32	16.97	20.29	24.65	30.92	44.39
	diff	0.39	1.09	3.39	6.31	9.29	12.56	16.42	20.58	24.56	28.52	33.03	39.30	48.51	67.14
NMAD (m)	E	2.26	2.59	3.91	5.41	6.91	8.49	10.32	12.41	14.62	17.24	21.44	27.52	35.15	49.74
	ENE	2.27	2.61	3.91	5.36	6.72	8.16	9.80	11.67	13.66	16.13	20.00	24.53	30.32	39.31
	NE	2.30	2.67	3.85	5.09	6.17	7.23	8.40	9.82	11.48	13.80	16.97	21.03	26.48	37.93
	NNE	2.37	2.72	3.78	4.82	5.69	6.41	7.17	8.06	9.33	11.33	14.41	18.47	24.77	36.73
	N	2.47	2.77	3.77	4.78	5.63	6.30	6.92	7.65	8.80	10.58	13.54	17.80	24.30	36.48
	NNW	2.54	2.81	3.89	5.12	6.23	7.14	8.01	8.97	10.29	12.23	15.62	19.49	25.88	38.41
	NW	2.59	2.82	4.11	5.69	7.15	8.50	9.84	11.30	13.04	15.44	18.78	22.91	27.81	37.86
	WNW	2.61	2.81	4.27	6.11	7.83	9.48	11.22	13.30	15.69	18.78	22.47	26.08	30.76	39.75
	W	2.62	2.79	4.30	6.16	7.92	9.69	11.63	13.90	16.63	20.19	24.57	29.46	35.75	46.24
	WSW	2.60	2.74	4.17	5.88	7.45	9.04	10.82	12.94	15.36	18.71	22.90	28.26	36.94	50.71
	SW	2.57	2.70	3.97	5.36	6.65	7.84	9.17	10.81	12.70	15.49	18.95	23.56	30.23	44.84
	SSW	2.52	2.69	3.73	4.89	5.85	6.69	7.56	8.60	10.06	12.46	15.47	19.56	24.77	37.01
	S	2.48	2.68	3.60	4.61	5.48	6.15	6.82	7.58	8.98	11.19	14.28	18.23	24.07	36.07
	SSE	2.39	2.66	3.60	4.66	5.61	6.41	7.27	8.25	9.74	11.86	14.93	19.03	24.73	39.13
	SE	2.34	2.63	3.70	4.92	6.10	7.19	8.45	9.96	11.72	14.03	17.13	21.39	27.59	42.38
	ESE	2.30	2.60	3.83	5.23	6.63	8.07	9.71	11.71	13.82	16.46	20.10	25.32	34.40	50.33
	All	2.44	2.73	4.15	5.87	7.59	9.40	11.51	13.94	16.51	19.41	23.40	28.59	35.59	48.80
	min	2.26	2.59	3.60	4.61	5.48	6.15	6.82	7.58	8.80	10.58	13.54	17.80	24.07	36.07
	max	2.62	2.82	4.30	6.16	7.92	9.69	11.63	13.90	16.63	20.19	24.57	29.46	36.94	50.71
	diff	0.36	0.23	0.70	1.55	2.44	3.54	4.81	6.32	7.83	9.61	11.02	11.65	12.86	14.64

Table S5: Detailed robust statistics of CEM according to variation in both slope and aspect.

		Slope (degrees)													
	Aspect	0-1	1-5	5-10	10-15	15-20	20-25	25-30	30-35	35-40	40-45	45-50	50-55	55-60	>60
Ncells (10^6)	All	117.740	122.149	38.674	21.460	16.420	13.470	10.737	7.909	4.603	1.901	0.745	0.332	0.162	0.129
MAE (m)	E	3.09	3.69	5.00	5.85	6.62	7.47	8.61	10.13	12.05	14.35	17.56	21.84	27.04	39.27
	ENE	3.07	3.66	5.02	5.90	6.68	7.48	8.54	10.05	11.92	14.27	17.18	21.30	26.28	39.65
	NE	3.10	3.73	5.05	5.93	6.68	7.41	8.33	9.64	11.26	13.52	16.89	21.29	27.20	40.65
	NNE	3.16	3.83	5.08	5.92	6.61	7.28	8.03	9.10	10.54	12.83	16.24	21.16	27.00	41.79
	N	3.24	3.90	5.09	5.92	6.63	7.27	7.98	8.94	10.25	12.39	15.46	20.15	25.90	39.79
	NNW	3.27	3.93	5.10	5.96	6.75	7.47	8.24	9.18	10.48	12.63	15.72	20.04	25.15	38.46
	NW	3.29	3.92	5.10	6.04	6.92	7.84	8.81	9.83	11.26	13.46	16.58	20.14	24.83	38.85
	WNW	3.30	3.87	5.12	6.14	7.12	8.19	9.34	10.67	12.20	14.37	16.95	20.24	25.47	37.33
	W	3.32	3.83	5.12	6.17	7.20	8.33	9.58	10.94	12.53	14.47	17.09	20.26	25.54	40.11
	WSW	3.32	3.80	5.10	6.10	7.06	8.16	9.38	10.61	11.98	13.92	16.40	19.74	24.06	36.87
	SW	3.30	3.84	5.06	5.93	6.76	7.70	8.76	9.89	11.18	13.03	15.31	18.31	22.72	34.12
	SSW	3.23	3.90	5.01	5.78	6.44	7.15	8.06	9.15	10.34	12.24	14.94	17.89	22.70	35.32
	S	3.25	3.92	4.97	5.67	6.26	6.88	7.60	8.51	9.64	11.57	14.42	18.02	22.91	37.78
	SSE	3.22	3.93	4.95	5.59	6.20	6.81	7.49	8.34	9.56	11.53	14.61	18.37	23.41	40.70
	SE	3.20	3.90	4.97	5.68	6.34	7.05	7.87	8.87	10.32	12.42	15.64	19.30	24.83	44.32
	ESE	3.14	3.80	4.99	5.78	6.51	7.33	8.36	9.74	11.47	13.71	16.71	20.77	25.52	39.65
	All	3.21	3.83	5.04	5.90	6.68	7.50	8.44	9.59	11.04	13.14	16.08	19.96	25.12	39.19
	min	3.07	3.66	4.95	5.59	6.20	6.81	7.49	8.34	9.56	11.53	14.42	17.89	22.70	34.12
	max	3.32	3.93	5.12	6.17	7.20	8.33	9.58	10.94	12.53	14.47	17.56	21.84	27.20	44.32
	diff	0.25	0.27	0.17	0.59	1.01	1.53	2.09	2.61	2.97	2.94	3.14	3.94	4.50	10.19
Median (m)	E	-0.49	-0.51	0.44	1.71	2.81	3.97	5.30	6.92	8.71	10.30	12.37	14.80	17.56	24.97
	ENE	-0.50	-0.50	0.38	1.56	2.51	3.47	4.62	6.10	7.95	9.45	10.94	13.65	16.44	22.81
	NE	-0.48	-0.57	0.16	1.06	1.77	2.45	3.40	4.77	6.42	7.64	9.27	11.23	13.73	19.13
	NNE	-0.46	-0.62	-0.23	0.33	0.66	1.01	1.65	2.77	3.99	4.99	6.24	8.15	10.19	16.06
	N	-0.45	-0.72	-0.64	-0.48	-0.57	-0.70	-0.54	0.03	0.79	1.60	2.77	4.04	6.15	11.64
	NNW	-0.42	-0.78	-1.00	-1.30	-1.80	-2.37	-2.83	-2.95	-2.65	-2.30	-1.68	-0.18	1.81	6.45
	NW	-0.35	-0.84	-1.34	-2.04	-2.92	-3.92	-4.90	-5.65	-6.08	-6.22	-5.92	-4.61	-2.50	2.64
	WNW	-0.32	-0.89	-1.61	-2.55	-3.67	-4.99	-6.35	-7.61	-8.52	-9.02	-9.23	-8.80	-6.82	-1.41
	W	-0.31	-0.92	-1.73	-2.76	-3.95	-5.39	-6.78	-8.05	-9.21	-9.95	-10.60	-10.60	-10.16	-4.66
	WSW	-0.35	-0.89	-1.67	-2.59	-3.70	-5.01	-6.40	-7.58	-8.53	-9.44	-10.33	-10.90	-11.85	-10.04
	SW	-0.38	-0.83	-1.43	-2.07	-2.88	-3.90	-5.08	-6.21	-6.98	-7.86	-8.48	-9.52	-10.55	-10.65
	SSW	-0.40	-0.80	-1.11	-1.35	-1.81	-2.41	-3.25	-4.17	-4.76	-5.31	-5.98	-6.90	-8.41	-10.93
	S	-0.42	-0.77	-0.70	-0.47	-0.42	-0.55	-1.01	-1.36	-1.36	-1.60	-2.00	-2.28	-2.59	-0.15
	SSE	-0.45	-0.73	-0.24	0.44	0.99	1.35	1.54	1.80	2.41	2.88	3.42	3.79	5.65	12.75
	SE	-0.49	-0.64	0.15	1.24	2.13	2.95	3.74	4.67	5.89	6.86	8.05	9.93	12.49	20.25
	ESE	-0.50	-0.54	0.37	1.64	2.71	3.86	5.05	6.62	8.21	9.62	11.20	13.69	15.77	22.04
	All	-0.43	-0.71	-0.65	-0.50	-0.54	-0.70	-0.79	-0.58	0.11	0.81	1.60	2.69	4.44	9.50
	min	-0.50	-0.92	-1.73	-2.76	-3.95	-5.39	-6.78	-8.05	-9.21	-9.95	-10.60	-10.90	-11.85	-10.93
	max	-0.31	-0.50	0.44	1.71	2.81	3.97	5.30	6.92	8.71	10.30	12.37	14.80	17.56	24.97
	diff	0.19	0.42	2.17	4.47	6.76	9.36	12.08	14.97	17.93	20.24	22.98	25.71	29.41	35.90
NMAD (m)	E	3.08	3.88	5.48	6.08	6.65	7.19	7.94	8.89	9.98	11.77	14.54	18.32	22.82	32.53
	ENE	3.05	3.85	5.48	6.12	6.73	7.35	8.10	9.08	10.17	12.18	15.02	18.28	22.85	33.58
	NE	3.04	3.91	5.49	6.23	6.93	7.63	8.43	9.31	10.29	12.25	15.28	19.13	24.37	36.23
	NNE	3.08	4.02	5.49	6.29	7.02	7.79	8.64	9.53	10.56	12.69	15.76	19.96	25.38	38.71
	N	3.12	4.06	5.44	6.28	7.10	7.96	8.92	10.01	11.10	13.29	16.10	20.77	26.71	39.60
	NNW	3.17	4.08	5.37	6.20	7.01	7.87	8.90	10.03	11.42	13.65	16.84	21.40	27.52	40.38
	NW	3.20	4.07	5.29	6.07	6.81	7.66	8.61	9.71	11.17	13.63	16.86	21.01	26.65	41.48
	WNW	3.23	4.01	5.23	5.97	6.69	7.41	8.21	9.25	10.62	12.94	16.23	19.67	25.74	37.26
	W	3.26	3.96	5.21	5.92	6.60	7.32	8.14	9.08	10.29	12.32	15.05	18.57	24.46	37.61
	WSW	3.25	3.95	5.21	5.92	6.57	7.29	8.12	8.94	9.98	11.93	14.41	17.35	22.83	34.13
	SW	3.21	4.01	5.25	5.94	6.60	7.35	8.17	8.97	10.10	11.92	14.32	17.17	21.71	32.03
	SSW	3.20	4.10	5.29	6.01	6.65	7.39	8.25	9.19	10.41	12.23	14.63	17.54	21.40	31.70
	S	3.19	4.14	5.36	6.07	6.75	7.57	8.48	9.50	10.69	12.62	15.21	18.78	23.20	36.11
	SSE	3.17	4.18	5.44	6.02	6.68	7.45	8.35	9.35	10.56	12.47	15.34	19.20	24.20	36.98
	SE	3.16	4.15	5.50	6.06	6.61	7.29	8.09	9.04	10.18	12.10	15.15	18.57	22.87	36.37
	ESE	3.12	4.04	5.50	6.08	6.60	7.17	7.88	8.74	9.80	11.75	14.67	18.03	22.61	32.39
	All	3.15	4.02	5.47	6.43	7.44	8.61	9.95	11.49	13.23	15.52	18.44	22.19	27.12	39.62
	min	3.04	3.85	5.21	5.92	6.57	7.17	7.88	8.74	9.80	11.75	14.32	17.17	21.40	31.70
	max	3.26	4.18	5.50	6.29	7.10	7.96	8.92	10.03	11.42	13.65	16.86	21.40	27.52	41.48
	diff	0.22	0.33	0.29	0.37	0.54	0.79	1.04	1.28	1.62	1.91	2.54	4.23	6.12	9.78

Table S6: Detailed robust statistics of GDEM3 according to variation in both slope and aspect.

		Slope (degrees)													
	Aspect	0-1	1-5	5-10	10-15	15-20	20-25	25-30	30-35	35-40	40-45	45-50	50-55	55-60	>60
Ncells (10^6)	All	117.654	122.067	38.647	21.442	16.404	13.454	10.718	7.882	4.570	1.875	0.726	0.317	0.149	0.106
MAE (m)	E	5.11	5.28	6.30	7.39	8.35	9.32	10.52	12.13	14.27	16.61	19.67	23.46	29.10	39.72
	ENE	5.04	5.23	6.42	7.53	8.49	9.47	10.67	12.42	14.78	17.21	20.56	25.16	30.80	43.93
	NE	5.03	5.11	6.33	7.51	8.49	9.47	10.64	12.44	14.92	17.52	21.12	25.90	31.92	45.22
	NNE	5.00	5.01	6.15	7.34	8.35	9.35	10.56	12.28	14.53	17.01	20.71	25.30	30.27	41.94
	N	5.03	4.98	5.97	7.14	8.13	9.12	10.23	11.76	13.82	16.12	19.52	23.64	27.54	39.70
	NNW	5.14	4.98	5.85	6.95	7.92	8.82	9.83	11.13	12.90	15.11	18.53	22.46	27.45	40.61
	NW	5.28	5.05	5.83	6.83	7.72	8.54	9.45	10.60	12.03	13.98	17.24	21.41	26.50	41.39
	WNW	5.32	5.10	5.84	6.72	7.51	8.22	9.01	10.08	11.25	12.95	15.72	19.42	24.63	36.49
	W	5.34	5.15	5.96	6.73	7.35	7.90	8.59	9.53	10.67	12.27	14.99	18.34	23.39	33.46
	WSW	5.30	5.16	6.01	6.72	7.26	7.77	8.38	9.25	10.36	12.10	14.82	18.54	23.17	33.65
	SW	5.25	5.12	5.87	6.63	7.26	7.81	8.42	9.18	10.31	12.07	14.96	18.54	23.49	34.59
	SSW	5.17	5.01	5.69	6.56	7.35	7.99	8.64	9.37	10.55	12.40	15.27	19.31	24.10	37.86
	S	5.14	4.94	5.59	6.54	7.42	8.19	8.90	9.66	10.91	12.68	15.51	19.70	24.75	37.98
	SSE	5.17	4.96	5.63	6.62	7.62	8.52	9.39	10.36	11.66	13.47	15.86	20.00	24.42	34.85
	SE	5.21	5.06	5.80	6.87	7.89	8.85	9.88	11.08	12.56	14.29	16.71	20.05	24.60	34.84
	ESE	5.17	5.17	6.01	7.10	8.11	9.09	10.25	11.70	13.40	15.39	17.90	21.65	26.00	36.24
	All	5.16	5.09	5.96	6.95	7.83	8.66	9.60	10.84	12.52	14.59	17.62	21.67	26.66	38.63
	min	5.00	4.94	5.59	6.54	7.26	7.77	8.38	9.18	10.31	12.07	14.82	18.34	23.17	33.46
	max	5.34	5.28	6.42	7.53	8.49	9.47	10.67	12.44	14.92	17.52	21.12	25.90	31.92	45.22
	diff	0.34	0.33	0.84	0.98	1.24	1.70	2.28	3.26	4.61	5.45	6.30	7.56	8.75	11.76
Median (m)	E	0.44	0.09	0.28	0.66	1.21	1.68	2.15	2.68	3.09	2.84	2.06	0.39	0.52	1.78
	ENE	0.37	0.08	0.10	0.42	0.91	1.40	1.82	2.60	3.46	2.89	1.80	0.96	2.24	4.86
	NE	0.59	0.18	0.08	0.29	0.67	1.04	1.58	2.63	3.65	2.91	1.44	1.30	2.25	7.92
	NNE	0.90	0.23	0.03	-0.01	0.14	0.44	1.03	2.23	3.18	2.26	1.10	2.03	3.70	10.28
	N	1.28	0.27	-0.04	-0.34	-0.45	-0.36	0.21	1.29	2.20	1.79	1.00	1.99	4.25	12.93
	NNW	1.42	0.34	-0.06	-0.49	-0.78	-0.81	-0.23	0.69	1.57	1.55	1.82	3.37	7.84	17.43
	NW	1.63	0.43	0.00	-0.48	-0.80	-0.88	-0.46	0.37	1.16	1.42	2.60	5.69	9.35	20.29
	WNW	1.63	0.35	0.00	-0.40	-0.62	-0.65	-0.31	0.33	0.83	1.09	1.93	3.81	6.50	14.31
	W	1.58	0.23	-0.19	-0.45	-0.47	-0.41	-0.14	0.31	0.52	0.09	-0.06	0.09	0.49	3.09
	WSW	1.34	0.27	-0.23	-0.30	-0.20	-0.05	0.24	0.65	0.67	0.00	-1.18	-2.30	-3.77	-8.49
	SW	1.22	0.42	-0.03	0.05	0.30	0.54	0.87	1.25	1.32	0.33	-1.40	-3.41	-5.98	-12.14
	SSW	1.16	0.32	0.20	0.38	0.70	0.94	1.20	1.57	1.51	0.35	-1.53	-3.68	-6.55	-14.65
	S	1.15	0.18	0.36	0.67	0.98	1.17	1.29	1.51	1.69	0.94	-0.89	-2.84	-6.04	-11.62
	SSE	0.93	0.17	0.53	0.97	1.31	1.54	1.83	2.07	2.39	1.99	0.42	-1.55	-3.78	-5.74
	SE	0.78	0.27	0.66	1.17	1.63	1.98	2.37	2.64	2.93	2.55	1.62	0.77	-0.37	-1.08
	ESE	0.56	0.24	0.55	1.03	1.56	2.01	2.45	2.94	3.20	2.60	1.72	0.32	-0.38	0.07
	All	1.00	0.25	0.14	0.20	0.38	0.59	0.98	1.58	2.05	1.54	0.62	0.12	0.09	0.96
	min	0.37	0.08	-0.23	-0.49	-0.80	-0.88	-0.46	0.31	0.52	0.00	-1.53	-3.68	-6.55	-14.65
	max	1.63	0.43	0.66	1.17	1.63	2.01	2.45	2.94	3.65	2.91	2.60	5.69	9.35	20.29
	diff	1.26	0.34	0.88	1.66	2.43	2.89	2.91	2.63	3.13	2.92	4.14	9.37	15.90	34.94
NMAD (m)	E	6.13	6.16	7.41	8.61	9.59	10.63	11.92	13.71	16.21	19.07	22.64	26.69	33.14	44.25
	ENE	6.04	6.09	7.59	8.89	9.94	10.99	12.28	14.14	16.70	19.73	23.40	29.03	35.10	49.52
	NE	6.07	5.97	7.51	8.93	10.06	11.17	12.42	14.37	17.04	20.06	24.20	29.92	36.73	49.79
	NNE	6.04	5.89	7.30	8.74	9.96	11.15	12.53	14.43	16.95	19.70	23.95	29.32	35.00	46.19
	N	6.04	5.87	7.03	8.45	9.70	10.94	12.30	14.06	16.38	18.89	22.68	27.20	31.83	42.76
	NNW	6.17	5.85	6.86	8.17	9.41	10.58	11.86	13.34	15.27	17.75	21.54	25.87	30.89	41.28
	NW	6.36	5.92	6.80	8.02	9.13	10.20	11.35	12.64	14.13	16.26	19.73	24.02	28.74	41.21
	WNW	6.43	5.94	6.78	7.85	8.83	9.72	10.70	11.99	13.23	14.97	17.90	21.84	26.75	38.32
	W	6.44	5.95	6.90	7.81	8.55	9.23	10.06	11.17	12.53	14.24	17.30	21.06	26.20	36.95
	WSW	6.45	6.00	7.00	7.78	8.37	9.02	9.77	10.77	12.06	13.96	16.73	20.98	26.73	35.56
	SW	6.41	6.02	6.88	7.65	8.29	8.92	9.62	10.52	11.79	13.77	16.71	20.87	25.88	34.85
	SSW	6.29	5.91	6.64	7.48	8.28	8.94	9.66	10.46	11.90	14.04	16.99	21.26	26.40	38.25
	S	6.20	5.83	6.47	7.38	8.24	9.04	9.84	10.72	12.18	14.27	17.22	21.84	27.18	39.21
	SSE	6.27	5.85	6.51	7.44	8.44	9.44	10.40	11.53	13.04	15.17	17.95	22.45	27.09	38.02
	SE	6.32	5.95	6.72	7.77	8.80	9.80	10.91	12.37	14.09	16.19	18.89	22.69	28.08	38.36
	ESE	6.26	6.08	7.01	8.15	9.18	10.19	11.43	13.11	15.07	17.49	20.20	24.72	29.76	40.92
	All	6.25	5.96	6.96	8.08	9.08	10.03	11.07	12.43	14.24	16.56	19.83	24.42	30.11	42.44
	min	6.04	5.83	6.47	7.38	8.24	8.92	9.62	10.46	11.79	13.77	16.71	20.87	25.88	34.85
	max	6.45	6.16	7.59	8.93	10.06	11.17	12.53	14.43	17.04	20.06	24.20	29.92	36.73	49.79
	diff	0.41	0.33	1.12	1.55	1.81	2.25	2.92	3.96	5.25	6.29	7.49	9.05	10.85	14.94

Table S7: Detailed robust statistics of GDEM2 according to variation in both slope and aspect.

		Slope (degrees)													
	Aspect	0-1	1-5	5-10	10-15	15-20	20-25	25-30	30-35	35-40	40-45	45-50	50-55	55-60	>60
Ncells (10^6)	All	117.719	122.099	38.641	21.433	16.396	13.448	10.714	7.885	4.580	1.885	0.735	0.325	0.157	0.122
MAE (m)	E	5.17	5.46	6.93	8.48	9.97	11.62	13.77	16.59	20.00	24.22	30.12	39.70	54.76	96.16
	ENE	5.12	5.51	7.05	8.51	9.87	11.27	13.05	15.58	18.82	22.25	26.79	32.76	41.23	56.64
	NE	5.13	5.56	7.19	8.80	10.28	11.78	13.65	16.53	20.26	23.57	28.08	35.18	42.64	59.07
	NNE	5.13	5.57	7.35	9.27	11.07	12.96	15.35	18.95	22.94	25.84	30.01	37.06	44.89	61.72
	N	5.19	5.60	7.52	9.76	11.85	14.10	17.03	21.11	25.66	28.72	32.43	38.09	44.61	62.49
	NNW	5.35	5.70	7.71	10.12	12.43	14.94	18.30	22.69	27.61	31.48	35.78	41.66	50.54	69.28
	NW	5.51	5.80	7.75	10.09	12.38	14.97	18.31	22.81	27.59	31.56	37.00	43.91	51.91	73.24
	WNW	5.52	5.72	7.45	9.49	11.55	13.87	16.85	20.78	24.76	28.35	32.94	38.61	45.84	62.76
	W	5.51	5.60	7.05	8.61	10.16	11.85	14.03	16.83	19.65	22.14	25.88	30.57	36.63	50.99
	WSW	5.41	5.52	6.80	7.94	8.99	10.05	11.37	13.14	15.09	17.02	20.26	24.80	30.64	45.78
	SW	5.32	5.49	6.59	7.66	8.59	9.48	10.54	11.96	13.79	16.48	20.71	26.33	33.52	52.20
	SSW	5.23	5.36	6.44	7.72	8.95	10.23	11.77	13.76	16.39	20.09	25.52	31.72	42.18	64.08
	S	5.22	5.29	6.41	7.98	9.71	11.68	14.13	16.93	20.13	24.31	30.02	37.89	47.76	73.55
	SSE	5.25	5.30	6.51	8.27	10.33	12.74	15.60	18.98	22.69	27.30	33.86	42.17	52.08	68.15
	SE	5.30	5.37	6.66	8.43	10.46	12.80	15.70	19.20	22.99	27.66	33.48	40.55	48.82	88.20
	ESE	5.24	5.42	6.79	8.46	10.23	12.26	14.89	18.17	21.93	26.83	33.60	41.96	53.09	91.49
	All	5.27	5.51	7.00	8.72	10.42	12.26	14.59	17.67	21.18	24.76	29.68	36.45	45.28	67.83
	min	5.12	5.29	6.41	7.66	8.59	9.48	10.54	11.96	13.79	16.48	20.26	24.80	30.64	45.78
	max	5.52	5.80	7.75	10.12	12.43	14.97	18.31	22.81	27.61	31.56	37.00	43.91	54.76	96.16
	diff	0.40	0.52	1.34	2.46	3.84	5.49	7.77	10.84	13.82	15.08	16.74	19.11	24.12	50.38
Median (m)	E	1.35	0.59	-0.52	-1.77	-2.91	-4.23	-5.79	-7.37	-8.75	-10.70	-13.35	-17.27	-19.17	-20.80
	ENE	1.36	1.02	0.57	0.25	0.10	-0.08	-0.34	-0.10	0.50	-0.66	-2.33	-3.67	-4.01	-2.72
	NE	1.60	1.58	1.97	2.63	3.50	4.41	5.56	7.54	9.53	9.28	8.40	8.69	9.24	14.78
	NNE	1.88	2.01	3.21	4.73	6.39	8.22	10.48	13.73	16.73	17.10	16.96	18.74	21.39	28.70
	N	2.25	2.29	4.10	6.26	8.45	10.87	13.95	17.98	21.94	23.56	24.18	26.89	31.16	43.50
	NNW	2.48	2.52	4.63	7.09	9.64	12.43	16.09	20.56	25.01	27.93	30.28	33.89	40.96	55.13
	NW	2.69	2.60	4.64	7.11	9.68	12.60	16.24	20.80	25.25	28.58	32.70	37.82	44.60	61.09
	WNW	2.69	2.32	3.96	6.07	8.40	11.06	14.37	18.42	22.21	25.28	28.80	33.10	38.25	49.93
	W	2.62	1.89	2.71	4.09	5.86	7.83	10.22	13.05	15.52	17.20	18.82	21.02	23.33	30.06
	WSW	2.35	1.54	1.42	1.82	2.59	3.58	4.68	5.99	6.83	6.72	5.84	4.70	4.13	0.26
	SW	2.14	1.30	0.31	-0.30	-0.56	-0.76	-0.94	-1.25	-1.87	-3.90	-6.82	-10.56	-14.81	-24.36
	SSW	2.01	0.83	-0.63	-2.12	-3.39	-4.82	-6.38	-8.13	-10.25	-13.21	-17.28	-21.70	-27.78	-42.57
	S	1.94	0.39	-1.34	-3.42	-5.53	-7.92	-10.68	-13.64	-16.50	-19.89	-24.22	-29.08	-35.11	-46.52
	SSE	1.73	0.23	-1.65	-3.97	-6.51	-9.29	-12.39	-15.90	-19.34	-22.94	-27.47	-32.33	-37.09	-45.10
	SE	1.62	0.31	-1.54	-3.72	-6.13	-8.84	-11.86	-15.46	-18.96	-22.70	-27.14	-31.46	-35.42	-39.93
	ESE	1.45	0.43	-1.19	-3.02	-4.91	-7.09	-9.63	-12.47	-15.26	-18.70	-22.76	-26.86	-30.09	-35.38
	All	1.95	1.32	1.16	1.16	1.37	1.65	2.08	2.71	3.11	1.79	-0.28	-1.55	-2.64	-4.38
	min	1.35	0.23	-1.65	-3.97	-6.51	-9.29	-12.39	-15.90	-19.34	-22.94	-27.47	-32.33	-37.09	-46.52
	max	2.69	2.60	4.64	7.11	9.68	12.60	16.24	20.80	25.25	28.58	32.70	37.82	44.60	61.09
	diff	1.34	2.37	6.30	11.08	16.18	21.89	28.62	36.70	44.59	51.52	60.18	70.15	81.69	107.61
NMAD (m)	E	5.98	6.27	8.02	9.60	11.06	12.66	14.75	17.49	20.87	24.63	29.03	34.98	43.42	59.38
	ENE	5.91	6.27	8.20	9.88	11.46	13.06	15.19	18.01	21.66	25.30	29.50	35.75	44.32	60.97
	NE	5.89	6.26	8.20	9.96	11.49	13.02	14.96	17.74	21.19	24.87	29.54	36.45	44.45	62.45
	NNE	5.81	6.20	8.01	9.82	11.30	12.76	14.52	17.00	20.03	23.10	27.89	34.24	42.57	60.21
	N	5.73	6.15	7.83	9.62	11.06	12.46	14.06	16.20	18.74	21.50	25.32	31.01	36.87	52.56
	NNW	5.86	6.22	7.84	9.59	11.02	12.37	13.87	15.66	17.74	20.16	23.61	28.68	34.99	49.03
	NW	6.01	6.30	7.92	9.61	11.02	12.38	13.87	15.62	17.42	19.43	22.83	27.55	32.95	48.81
	WNW	6.05	6.26	7.85	9.45	10.85	12.17	13.66	15.45	17.33	19.10	22.52	26.71	32.19	44.07
	W	6.07	6.18	7.79	9.29	10.57	11.78	13.17	15.00	16.87	19.02	22.61	26.91	32.74	45.27
	WSW	6.06	6.21	7.84	9.12	10.29	11.40	12.69	14.42	16.42	18.84	22.28	27.59	34.68	46.55
	SW	6.01	6.28	7.73	8.89	9.97	11.07	12.26	13.93	15.92	18.45	22.06	26.97	33.54	47.28
	SSW	5.92	6.23	7.49	8.58	9.65	10.67	11.86	13.44	15.57	18.18	21.42	26.41	32.24	47.68
	S	5.88	6.20	7.32	8.40	9.45	10.43	11.53	12.83	14.81	17.23	20.75	25.44	31.16	45.16
	SSE	6.00	6.23	7.36	8.50	9.62	10.71	11.87	13.44	15.29	17.72	20.95	25.95	30.67	44.42
	SE	6.09	6.28	7.57	8.85	10.10	11.29	12.77	14.73	16.95	19.38	22.49	26.73	33.09	47.51
	ESE	6.06	6.29	7.77	9.20	10.59	12.03	13.85	16.29	19.03	22.09	25.62	31.29	36.76	51.87
	All	5.98	6.30	8.20	10.33	12.49	14.91	17.95	21.90	26.18	30.23	35.23	42.19	50.68	69.39
	min	5.73	6.15	7.32	8.40	9.45	10.43	11.53	12.83	14.81	17.23	20.75	25.44	30.67	44.07
	max	6.09	6.30	8.20	9.96	11.49	13.06	15.19	18.01	21.66	25.30	29.54	36.45	44.45	62.45
	diff	0.36	0.14	0.88	1.56	2.04	2.63	3.66	5.18	6.85	8.07	8.79	11.00	13.77	18.38